Journal of Cosmology and Astroparticle Physics
An IOP and SISSA journal

Phantom scalar-tensor models and cosmological tensions

Mario Ballardini,[a,b,c] **Angelo Giuseppe Ferrari**[d,e] **and Fabio Finelli**[c,e]

[a]Dipartimento di Fisica e Scienze della Terra, Università degli Studi di Ferrara, via Giuseppe Saragat 1, Ferrara 44122, Italy
[b]INFN, Sezione di Ferrara, via Giuseppe Saragat 1, Ferrara 44122, Italy
[c]INAF/OAS Bologna, via Piero Gobetti 101, Bologna 40129, Italy
[d]Dipartimento di Fisica e Astronomia, Università di Bologna, viale Berti Pichat 6/2, Bologna 40127, Italy
[e]INFN, Sezione di Bologna, viale C. Berti Pichat 6/2, Bologna 40127, Italy

E-mail: mario.ballardini@unife.it, angelo.ferrari3@unibo.it, fabio.finelli@inaf.it

Received February 20, 2023
Revised March 14, 2023
Accepted March 14, 2023
Published April 11, 2023

Abstract. We study three different extended scalar-tensor theories of gravity by also allowing a negative sign for the kinetic term for the scalar field in the Jordan frame. Our scope is to understand how the observational constraints for these models cope with the volume of the parameter space in which the theory is healthy. Models with a negative kinetic term lead to decreasing effective gravitational constant with redshift and behave as an effective relativistic component with a negative energy density as opposite to their corresponding version with a standard kinetic term. As a consequence, we find that the extended branch with a negative sign for the kinetic term correspond in general to lower H_0 and σ_8 compared to ΛCDM. We find that in all the cases with a negative sign for the kinetic term studied here, cosmological observations constrain these models around GR and prefer a volume of the parameter space in which the theory is not healthy since the scalar field behave as a ghost also in the related Einstein frame. We show that also in the phantom branch early modify gravity with a quartic coupling can substantially reduce the H_0 tension fitting the combination of cosmic microwave background data from *Planck*, baryon acoustic oscillations from BOSS and eBOSS, and Supernovae from the Pantheon sample with calibration information by SH0ES.

Keywords: cosmological parameters from CMBR, Cosmological perturbation theory in GR and beyond, dark energy theory, modified gravity

ArXiv ePrint: 2302.05291

https://doi.org/10.1088/1475-7516/2023/04/029

Contents

1 Introduction

The ΛCDM model represents the current standard cosmological model providing an excellent fit to most of cosmological observations: measurements of luminosity distances of Type Ia Supernovae (SN Ia) [1–3], measurements of cosmic microwave background (CMB) anisotropies in temperature and polarization [4], measurements of the baryon acoustic oscillations (BAO) in galaxy and cluster distribution [5, 6], cosmic shear measurements of the CMB [7–9] and of the galaxy distribution [10, 11], and the predicted abundance of light elements [12]. While the ΛCDM model provides an accurate description to most of cosmological observations, it relies on a number of assumptions and unknown ingredients such dark matter, dark energy, and a suitable mechanism to produce its initial condition.

In addition to the interest in testing at which extent the validity of the ΛCDM model holds with better and more data, the theoretical search for extended models [13–21] has been fueled by the persisting cosmological tensions or rather intriguing inconsistencies between different measurements under the framework of the minimal ΛCDM model; see refs. [22–29] for reviews on the topic.

Among the many proposed models, there are still difficulties in finding a candidate able to completely solve the discrepancy between the value of the Hubble parameter inferred in ΛCDM using CMB data from the *Planck* DR3, i.e. $H_0 = (67.36 \pm 0.54)\,\mathrm{km\,s^{-1}\,Mpc^{-1}}$ at 68% confidence level (C.L.) [30], with the measurement from the SH0ES team [31] obtained with cosmic distance ladder calibration of SN Ia from the revised Pantheon+ compilation [3], i.e. $H_0 = (73.0 \pm 1.0)\,\mathrm{km\,s^{-1}\,Mpc^{-1}}$ at 68% C.L., once all cosmological data are combined.

It is even more difficult to reconcile the value of the Hubble parameter together with the persistent but less significant tension between *Planck* and galaxy shear experiments, quantified through the value of $S_8 \equiv \sigma_8\sqrt{\Omega_\mathrm{m}/0.3}$, see [27]. Adopting a flat ΛCDM model, cosmic shear analysis of the fourth data release of the *Kilo-Degree Survey* (KiDS-1000) reported $S_8 = 0.759^{+0.024}_{-0.021}$ [10] and $S_8 = 0.776 \pm 0.017$ from *Dark Energy Survey* (DES) Year 3 (Y3) combination of three large-scale structures (LSS) two-point correlation functions (3×2 pt) [11], while the value measured by *Planck* corresponds to $S_8 = 0.832 \pm 0.013$ [30]. Indeed, while minimally and nonminimally coupled scalar field have been extensively studied as possible solutions to the Hubble tension, they usually lead to a higher value of the Hubble constant together with a larger growth of structures on small scales, i.e. a higher value of σ_8, see refs. [13, 14, 32–36]. However, they generally predict a value of S_8 compatible to the one obtained in ΛCDM avoiding to exacerbate the tension on the growth of structure amplitude since the larger σ_8 is compensated by a larger value of H_0 and a lower value of Ω_m [20, 37–39].

One possibility is to extend the dynamics of the scalar field to behave differently at early- and late-time in order to solve both tensions at the same time. The possibility to have models with phenomenology in both the early and late universe has been tried in the context of modified gravity [20, 38], early dark sector [40], and combining modified gravity or early dark energy to extended neutrino physics [19, 41, 42].

In this paper, we study modified gravity models with a nonminimally coupled scalar field with negative kinetic energy, so-called *phantom* field. Note that this is not strictly related to the phantom dark energy models for which the dark energy (DE) equation of state can cross the *phantom divide* line $w_\mathrm{DE} = -1$. Moreover, scalar-tensor models can be realized with no necessity to introduce a ghost field [43] avoiding the problems in ghost phantom DE [44] to be plagued by classical and quantum instabilities [45]. Such a the non-canonical kinetic energy term can occur in supergravity models [46] and in higher derivative theories of gravity [47]. We show how a nonminimally coupled scalar field with the negative sign of its kinetic term (phantom branch) behaves differently compared to the case with standard kinetic term (standard branch) and we derive the constraints on these models combining the information from *Planck* 2018 DR3 CMB temperature, polarization and lensing, together with a compilation of BAO measurements from the releases DR7 and DR12 of the *Baryon Oscillation Spectroscopic Survey* (BOSS) and Lyα measurements from the *extended Baryon Oscillation Spectroscopic Survey* (eBOSS), and uncalibrated SN Ia from the Pantheon sample.

The paper is organized as follows. After this introduction, we describe the implementation of the various basic quantities in the context of scalar-tensor theories in section 2. In section 3, we describe the datasets and prior considered and we discuss our results for the three models studies: induced gravity, non-minimal coupling, and early modified gravity. In section 4 we draw our conclusions. In appendix A, we collect the tables with the constraints on all the cosmological parameters obtained with our MCMC analysis. Background equations, linear perturbations, and initial conditions for background and cosmological fluctuations are collected in appendices B–D. In appendix E, we present a comparison of the results by using CMB data plus different combinations of LSS measurements.

2 Theory and cosmological background dynamics

We study the action for the scalar-tensor theory in Jordan frame [48] which is given by

$$\mathcal{S} = \int \mathrm{d}^4x\sqrt{|g|}\left[\frac{F(\sigma)R}{2} - \frac{Z(\sigma)}{2}(\partial\sigma)^2 - V(\sigma) + \mathcal{L}_m\right] \tag{2.1}$$

where $|g|$ is the absolute value of the determinant of the metric $g_{\mu\nu}$, σ is the scalar field, $F(\sigma)$ is the non-minimal coupling function, R is the Ricci scalar, $V(\sigma)$ is the potential for σ, and $\mathcal{L}_m$ the Lagrangian density of matter minimally coupled to the metric (without introducing any direct coupling between the scalar field and the matter content we guarantee that the weak equivalence principle is exactly satisfied). The function $Z(\sigma)$ in front of the kinetic term can be set to ± 1 by a redefinition of the scalar field.

In this model, the effective gravitational constant $G_{\rm eff}$ for the attraction between two test masses [having the same physical meaning as the Newton gravitational constant in general relativity (GR)] is given by

$$G_{\rm eff} = \frac{1}{8\pi F}\frac{ZF + 2F_\sigma^2}{ZF + \frac{3}{2}F_\sigma^2} \tag{2.2}$$

on all scales for which the scalar field is effectively massless [43], i.e. $V_\sigma \simeq 0$ and $V_{\sigma\sigma} \simeq 0$.

The current values of the time derivative and field derivative of coupling F in these theories — assuming a homogeneous evolution of the scalar field for all the scales — are strongly constrained by Solar System tests of post-Newtonian parameters (for these quantities, we drop here the subscript 0)

$$\gamma_{\rm PN} = 1 - \frac{F_\sigma^2}{ZF + 2F_\sigma^2} \tag{2.3}$$

$$\beta_{\rm PN} = 1 + \frac{1}{4}\frac{FF_\sigma}{2ZF + 3F_\sigma^2}\frac{{\rm d}\gamma_{\rm PN}}{{\rm d}\sigma} \tag{2.4}$$

as well as the time variation of the effective cosmological constant. Current constraints [49–52] correspond to

$$\gamma_{\rm PN} - 1 = (2.1 \pm 2.3)\cdot 10^{-5} \tag{2.5}$$

$$\beta_{\rm PN} - 1 = (-4.1 \pm 7.8)\cdot 10^{-4} \tag{2.6}$$

$$\dot{G}/G = (7.1 \pm 7.6)\cdot 10^{-14}\,{\rm yr}^{-1}\,. \tag{2.7}$$

On cosmological scales, post-Newtonian parameters are weakly constrained from current cosmological data, see ref. [19], with the perspective to reach the Solar System accuracy with the combination of future cosmological surveys [38, 53, 54].

There are essentially two stability conditions which impact on these scalar-tensor theories. The condition

$$G_{\rm eff} > 0 \tag{2.8}$$

is one of the stability conditions of this theory meaning that the graviton is not a ghost. Moreover, we have the inequality

$$\frac{ZF}{F_\sigma^2} > -\frac{3}{2} \tag{2.9}$$

requiring the positivity of the kinetic energy of the scalar field in the Einstein frame [55]. Eqs. (2.8), (2.9) reduce to $ZFF_\sigma^{-2} > 0$ for $Z = +1$ or $-3/2 < ZFF_\sigma^{-2} < 0$ for $Z = -1$, and to $F > 0$. This condition can be mapped to a range of allowed parameter space for the parameters modelling $F(\sigma)$. However, we will consider a larger parameter space in the following analysis testing the models also for parameters violating the stability conditions in an agnostic way.

JCAP04(2023)029

3 Constraints and results

In this section, we present our constraints on the cosmological parameters of the models studied. In particular, we study the nonminimally coupling $F = \xi\sigma^2$, i.e. *induced gravity* (IG) [56, 57], and $F = N_{\rm Pl}^2 + \xi\sigma^2$ (hereafter NMC) both with a phantom scalar field, i.e. $Z = -1$; in both cases we consider $V(\sigma) = \lambda F^2(\sigma)/4$ which yields to an effectively massless dynamic [58, 59]. We study also the *early modified gravity* (EMG) model proposed in ref. [20] extended to $Z = -1$. This last case is given by $F = M_{\rm Pl}^2 + \xi\sigma^2$ and $V = \Lambda + \lambda\sigma^4/4$ with a negative amplitude λ of the self-interaction term in order to produce the peculiar evolution of the scalar field damped into coherent oscillations within the phantom branch. We perform a Markov-chain Monte Carlo (MCMC) analysis using a modified version of the `CLASSig` code [13], based on the Einstein-Boltzmann code `CLASS`[1] [60, 61], interfaced to the publicly sampling code `MontePython`[2] [62, 63]. The datasets used in this work include

- P18 refers to the CMB temperature, polarization, and lensing from *Planck* DR3 [64, 65].
- FS refers to the combination of pre-reconstructed full-shape monopole and quadrupole galaxy power spectra for three different sky-cuts CMASS NGC, CMASS SGC and LOWZ NGC [66] based on the publicly available code `PyBird`[3][67].
- BAO refers to the post-reconstruction measurements from BOSS DR12 [68], low-z BAO measurements from SDSS DR7 6dF and MGS [69, 70], Lyα BAO measurements from eBOSS, and combination of those [71–73].
- SN refers to the Pantheon catalogue of high-redshift supernovae, spanning the redshift range $0.01 < z < 2.3$ [74].[4]
- Additional constraints of a Gaussian prior on the density of baryons (hereafter BBN) motivated from Big Bang nucleosynthesis (BBN) constraints corresponding to $\omega_{\rm b} = 0.02235 \pm 0.0005$ [12], used in combination to FS and SN for the CMB-independent analysis.
- Additional constraints that include a Gaussian prior on the Hubble constant [hereafter $p(H_0)$], $H_0 = (73.04 \pm 1.04)\,{\rm km\,s^{-1}\,Mpc^{-1}}$ at 68% C.L., from ref. [31].

We vary 6 standard parameters, i.e. $\omega_{\rm b}$, $\omega_{\rm c}$, H_0, τ, $\ln\left(10^{10}A_{\rm s}\right)$, $n_{\rm s}$, and the modified gravity parameters. We assume 2 massless neutrino with $N_{\rm ur} = 2.0328$, and a massive one with fixed minimum mass $m_\nu = 0.06\,{\rm eV}$. We fix the primordial ^{4}He mass fraction $Y_{\rm p}$ according to the prediction from `PArthENoPE` [75, 76], by taking into account the relation with the baryon fraction $\omega_{\rm b}$ and the varying gravitational constant which enters in the Friedman equation during nucleosynthesis.

Following the minimization method of ref. [27], we report for each combination of datasets the $\Delta\chi^2$ values calculated with respect to the ΛCDM model where negative values correspond to a better fit of the dataset.

[1] https://github.com/lesgourg/class_public.
[2] https://github.com/brinckmann/montepython_public.
[3] https://github.com/pierrexyz/pybird/.
[4] https://github.com/dscolnic/Pantheon.

JCAP04(2023)029

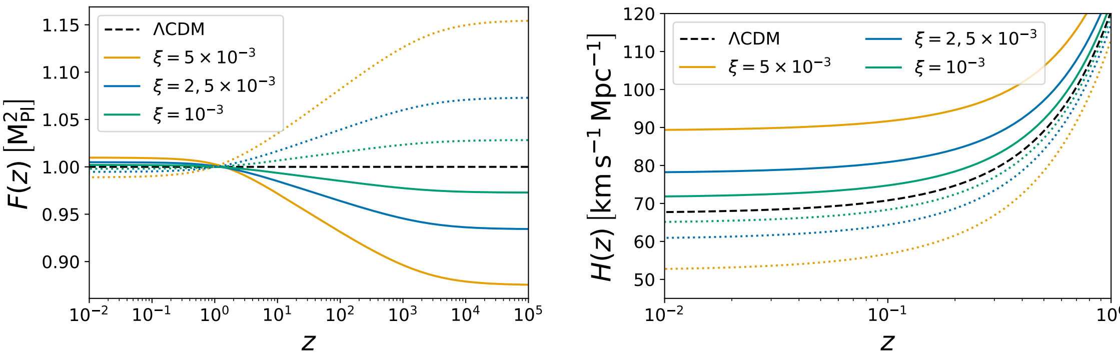

Figure 1. Time evolution of the coupling to the Ricci scalar $F = \xi\sigma^2$ (left panel) and of the Hubble parameter (right panel) for different values of the coupling parameter ξ in the standard branch (solid lines) and in the phantom one (dashed lines) for IG ($F = \xi\sigma^2,\ V = \lambda F^2/4$).

3.1 Phantom induced gravity

For IG (or equivalently extended Jordan-Brans-Dicke), with coupling $F(\sigma) = \xi\sigma^2$, we sample on the quantity $\zeta_{\rm IG} \equiv \ln(1 + 4\xi)$ which corresponds to a linear prior on the coupling to the parameter ξ for $\xi \ll 1$. Here we impose the following boundary condition on the current value of the effective gravitational constant

$$G_{\rm eff}(z = 0) = G \tag{3.1}$$

which fixes the final value of the scalar field.

Scalar-tensor theories of gravity such as extended Jordan-Brans-Dicke models, lead to a modification of the Hubble parameter H_0 due to the time evolution of σ and due to the redshift evolution of the gravitational strength. Indeed, a variation of the strength of gravity can be connected to a change of the expansion rate of the universe as

$$\frac{H(\xi \neq 0)}{H(\xi = 0)} \approx \sqrt{\frac{M_{\rm Pl}^2}{F(\sigma)}}\,. \tag{3.2}$$

For a fixed matter content, reducing the Planck mass $F(\sigma) < M_{\rm Pl}^2$ with respect to the GR prediction increases the expansion rate at a given time and consequently reduces the comoving sound horizon at recombination

$$r_s = \int_{z_*}^{\infty} {\rm d}z' \frac{c_{\rm s}(z')}{H(z')} \tag{3.3}$$

where z_* is the redshift parameter at recombination and $c_{\rm s}$ is the speed of sound in the photon-baryon fluid. We show in figure 1 that the coupling function increases in the branch with standard kinetic term (solid lines) while decreasing in the phantom branch (dashed lines). This different behaviour is connected with a different late-time evolution of the Hubble parameter (when the scalar field starts to evolve driven by the non-relativistic matter) which is larger than the ΛCDM case in the standard branch and lower in the phantom branch. This effect induces also a modification on the comoving angular diameter distance

$$D_{\rm M}(z) = \int_0^z \frac{{\rm d}z'}{H(z')} \tag{3.4}$$

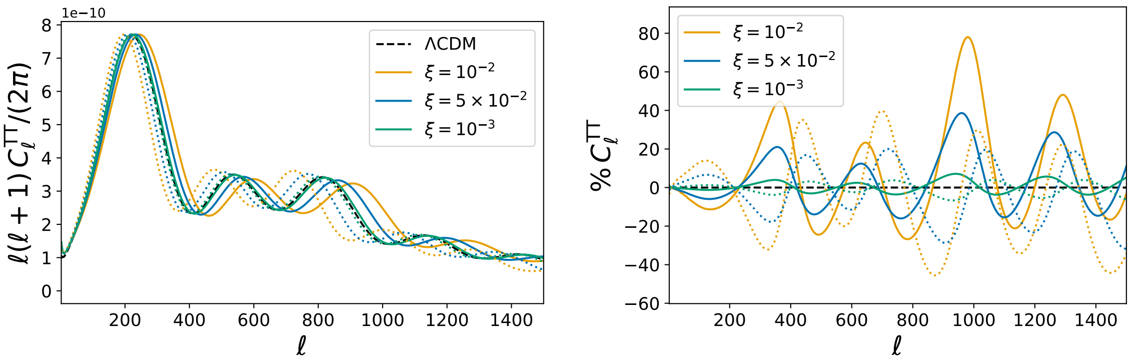

Figure 2. CMB temperature anisotropies power spectrum (left panel) and relative differences with respect to the ΛCDM case (right panel) for different values of the coupling parameter ξ in the standard branch (solid lines) and in the phantom one (dashed lines) for IG ($F = \xi\sigma^2,\ V = \lambda F^2/4$).

and does not cancel out on the angular size of horizon at the last-scattering surface θ_*

$$\theta_* = \frac{r_s}{D_{\rm M}(z_*)} \tag{3.5}$$

driving a shift on the acoustic peaks of the CMB connected to the evolution of the coupling F [19, 77, 78]. In figure 2, we show the shift of the acoustic peaks of the CMB temperature anisotropies angular power spectrum imprinted by the evolving effective Planck mass. The peaks move to the right in the positive branch and to the left in the phantom one. Indeed, in order to compensate this shift (keeping nearly unchanged the value of the CDM density parameter) the two branches go in the direction of a larger or a smaller value of $\Omega_{\rm m}$ once the CMB data are included in the analysis, see figure 3. Therefore it is possible to break the degeneracy at background level between the scalar field σ and the density parameters by combining early- and late-time probes.

In figure 3, we compare the CMB-only constraints for IG in the phantom branch to the standard case. We see that the degeneracy direction in the ξ–H_0 plane changes orientation going from one case to the other according to eq. (3.2). It turns out that the phantom branch allows much larger values of the coupling ξ and predicts a lower value for the Hubble constant without any prospect to reduce the H_0 tension. It is interesting to note that the extension of our study to the phantom case strengthen the correspondence between the kinetic term and the spatial curvature: the standard (phantom) kinetic term shifts the position to the right (left) as a negative (positive) spatial curvature.

Finally, it is interesting to note that the matter density root mean square fluctuations σ_8 goes toward lower values in the phantom branch compared to both the standard branch and the ΛCDM model predictions, see figure 4. This behaviour can be understood studying the late-time solution of the perturbation equation for the matter density contrast in the linear regime, on sub-horizon scales

$$\delta_{\rm m}'' + \left(\frac{3}{a} + \frac{H'}{H}\right)\delta_{\rm m}' - \frac{G_{\rm eff}}{2GH^2}\frac{\rho_{\rm m}}{a^2}\delta_{\rm m} \simeq 0 \tag{3.6}$$

where primes are derivatives with respect to the scale factor a. By rewriting the Friedmann

JCAP04(2023)029

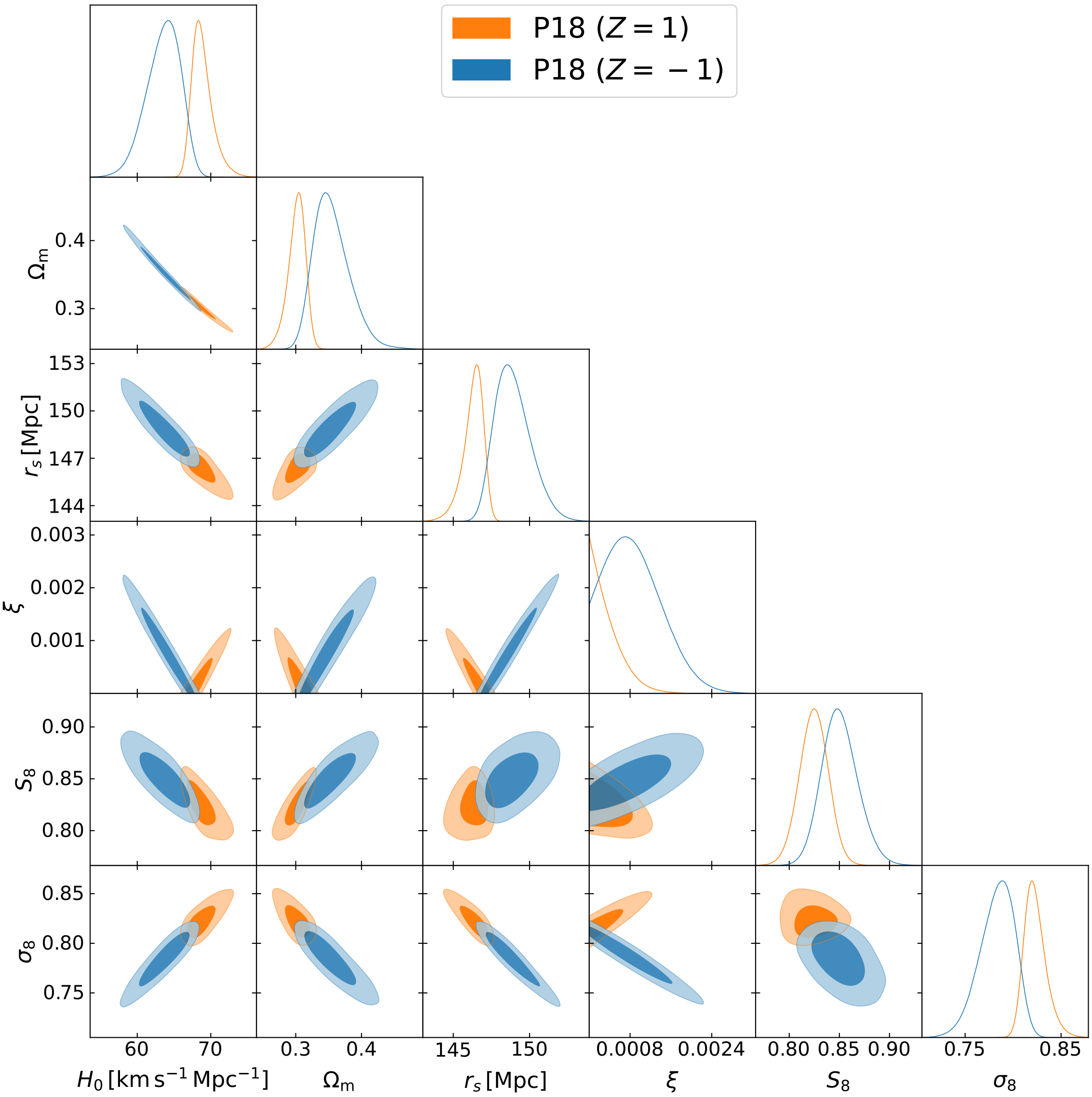

Figure 3. Marginalized joint 68% and 95% C.L. regions 2D parameter space using the CMB alone data for IG ($F = \xi\sigma^2,\ V = \lambda F^2/4$) with $Z = 1$ (orange) and for IG with $Z = -1$ (blue).

JCAP04(2023)029

equations (B.4), (B.5)

$$H^2 = \frac{\rho + V}{3F(1+f)} \tag{3.7}$$

$$\frac{H'}{H} = -\frac{3}{2a} - \frac{3}{2a}w - \frac{F'}{2F} - \frac{f'}{2(1+f)} \tag{3.8}$$

introducing the quantity

$$f = +a\frac{F_\sigma}{F}\sigma' - \frac{a^2 Z}{6F}\sigma'^2 \tag{3.9}$$

and where we used $\rho'/\rho = -3(1+w)/a$, we can write eq. (3.6) as

$$\delta''_{\rm m} + \left[\frac{3}{2a}(1-w) - \frac{F'}{2F} - \frac{f'}{2(1+f)}\right]\delta'_{\rm m} - \frac{3}{2a^2}\frac{2ZF + 4F_\sigma^2}{2ZF + 3F_\sigma^2}(1+f)\frac{\rho_{\rm m}}{\rho + V}\delta_{\rm m} \simeq 0\,. \tag{3.10}$$

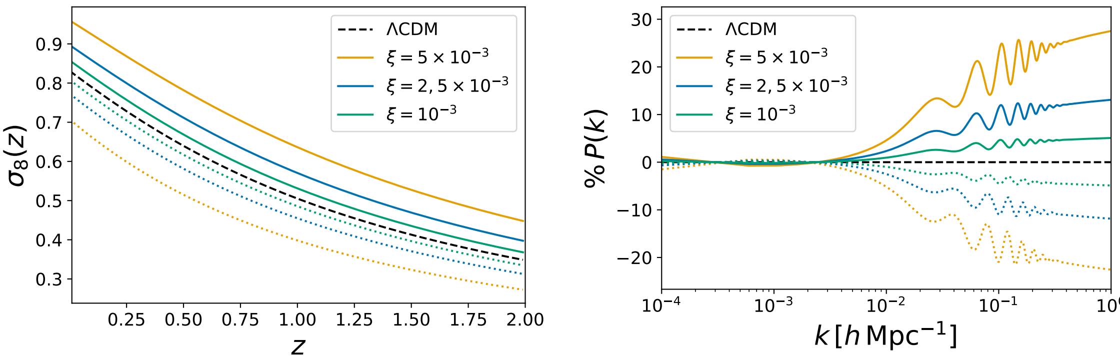

Figure 4. Time evolution of the amplitude of matter perturbation within spheres of radius $8\,h^{-1}\,\mathrm{Mpc}$ (left panel) and relative differences of the linear matter power spectrum at $z = 0$ with respect to ΛCDM (right panel) for different values of the coupling parameter ξ in the standard branch (solid lines) and in the phantom one (dashed lines) for IG ($F = \xi\sigma^2,\ V = \lambda F^2/4$).

During the matter-dominated era, the scalar field evolves as $\sigma \sim a^{2Z\xi}$ [59] leading for IG to

$$f \sim +\frac{10Z\xi}{3} \tag{3.11}$$

and consequently

$$\delta_{\mathrm{m}}'' + \frac{3}{2a}\left(1 - \frac{4Z\xi}{3}\right)\delta_{\mathrm{m}}' - \frac{3}{2a^2}\left(1 + \frac{16Z\xi}{3}\right)\delta_{\mathrm{m}} \simeq 0\,. \tag{3.12}$$

In the weak coupling regime for $\xi \ll 1$, which turns out to be the range allowed from observations, the leading-order growing solution of eq. (3.12) goes as $\delta_{\mathrm{m}} \sim a^{1+4Z\xi}$ showing a slower (faster) growth of structures compared to the ΛCDM case for $Z < 0$ ($Z > 0$) during the matter dominated era.

We show the results for most of the combination of datasets on figure 5 (in appendix E, we show a comparison between P18+BAO and P18+BAO+FS). The marginalized upper bound on the coupling parameter ξ at 95% C.L. corresponds to < 0.0024 for FS+SN, < 0.0018 for P18, < 0.00046 for P18+BAO, and < 0.00040 for P18+BAO+SN; see table 1 for the constraints on all the parameters.

In figure 5, we see the larger marginalized uncertainties for the analysis without CMB information, i.e. combining FS with SN and a Gaussian prior on ω_{b} motivated from BBN, and the analysis with CMB alone. In these cases larger value of ξ can be accommodated by changes in the density parameters and in the scalar spectral index.

The marginalized means and uncertainties for the Hubble constant H_0 $\left[\mathrm{km\,s^{-1}\,Mpc^{-1}}\right]$ at 68% C.L. correspond to 67.4 ± 1.8 for FS+SN, $63.6^{+2.7}_{-1.9}$ for P18, $67.17^{+0.64}_{-0.50}$ for P18+BAO, and $67.29^{+0.60}_{-0.47}$ for P18+BAO+SN; all of them are lower than the corresponding results we found in the standard branch, see refs. [19, 79]. The upper bound on ξ becomes much tighter, i.e. $\xi < 0.00016$ at 95% C.L., once we add a prior on H_0 in order to reproduce a larger value of the Hubble parameter, i.e. 68.34 ± 0.41 at 68% C.L., see figure 6 and table 4.

The marginalized constraint on the present value of σ_8 at 68% C.L. corresponds to 0.717 ± 0.049 for FS+SN, $0.784^{+0.021}_{-0.015}$ for P18, $0.799^{+0.010}_{-0.009}$ for P18+FS, and 0.8059 ± 0.0058 for P18+FS+SN. However, the combination $S_8 \equiv \sigma_8\sqrt{\Omega_{\mathrm{m}}/0.3}$, commonly used to quantify

JCAP04(2023)029

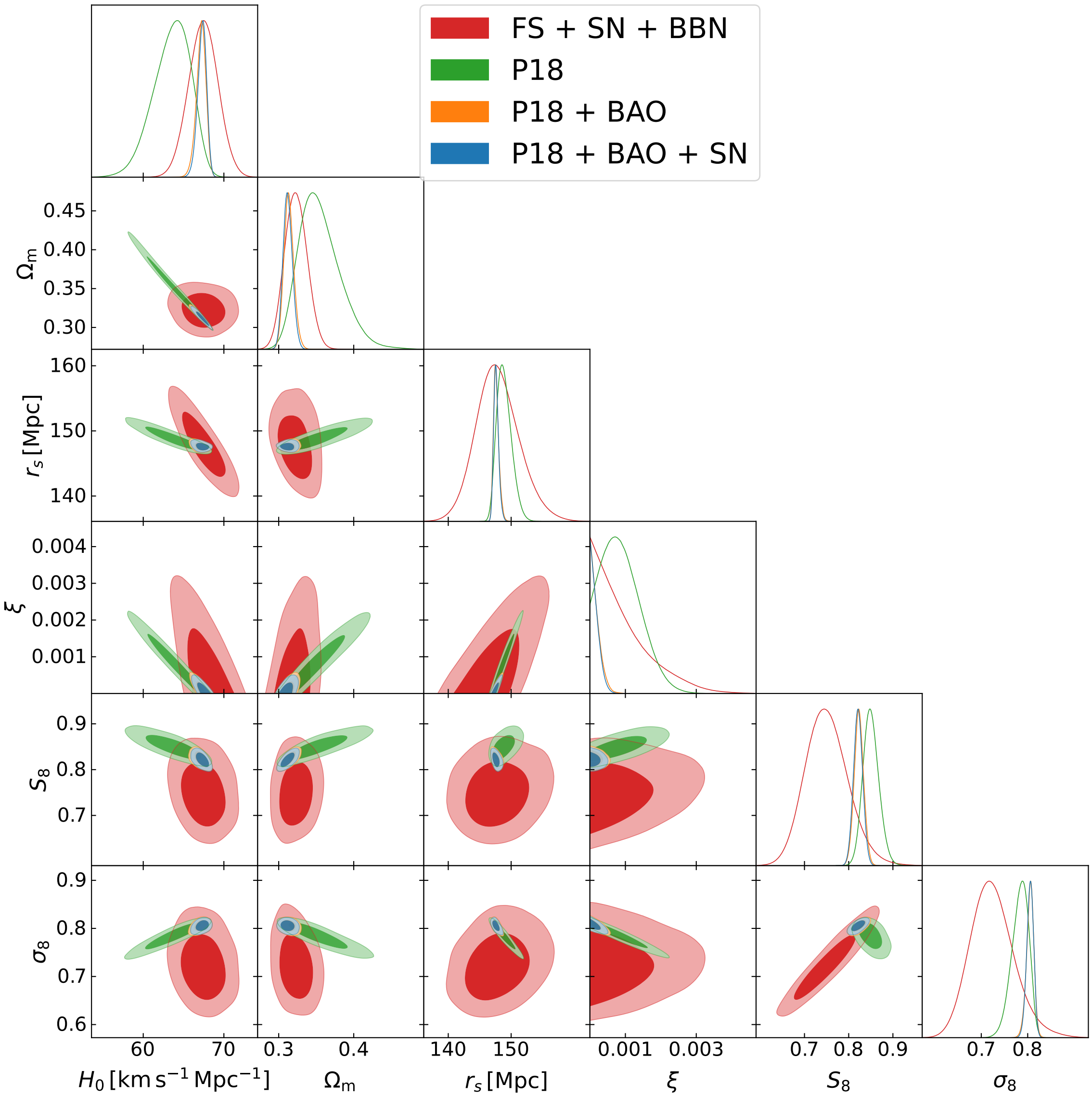

Figure 5. Marginalized joint 68% and 95% C.L. regions 2D parameter space using the CMB-independent combination FS+SN (red), P18 (green), the combination P18+BAO (orange), and the combination P18+BAO+SN (blue) for IG ($F = \xi\sigma^2$, $V = \lambda F^2/4$) in the phantom branch ($Z = -1$).

the tension between *Planck* and weak lensing of galaxies measurements, moves to the wrong direction. In order not to spoil the fit to CMB and galaxy measurements, an increase of the matter energy density is needed to compensate for the shifted position of the CMB acoustic peaks and of the BAO. Indeed, we find for S_8 0.744 ± 0.050 for FS+SN, $0.850^{+0.016}_{-0.019}$ for P18, $0.831^{+0.011}_{-0.012}$ for P18+FS, and 0.825 ± 0.012 for P18+FS+SN at 68% C.L., resulting to be larger than in the standard branch as shown in figure 3.

The constraints found are at odds with the parameter space free from ghost which corresponds for IG to $\xi > 1/6$ according to eqs. (2.8), (2.9). Note that, this condition for ξ can be relaxed if one considers a more general Lagrangian with respect to the one introduced in eq. (2.1). Higher order terms in the kinetic energy $X \equiv -\partial_\mu\sigma\partial^\mu\sigma/2$ [80] appear in low-energy effective string theory [81] or in tachyon condensation [82]. In a more general Lagrangian

JCAP04(2023)029

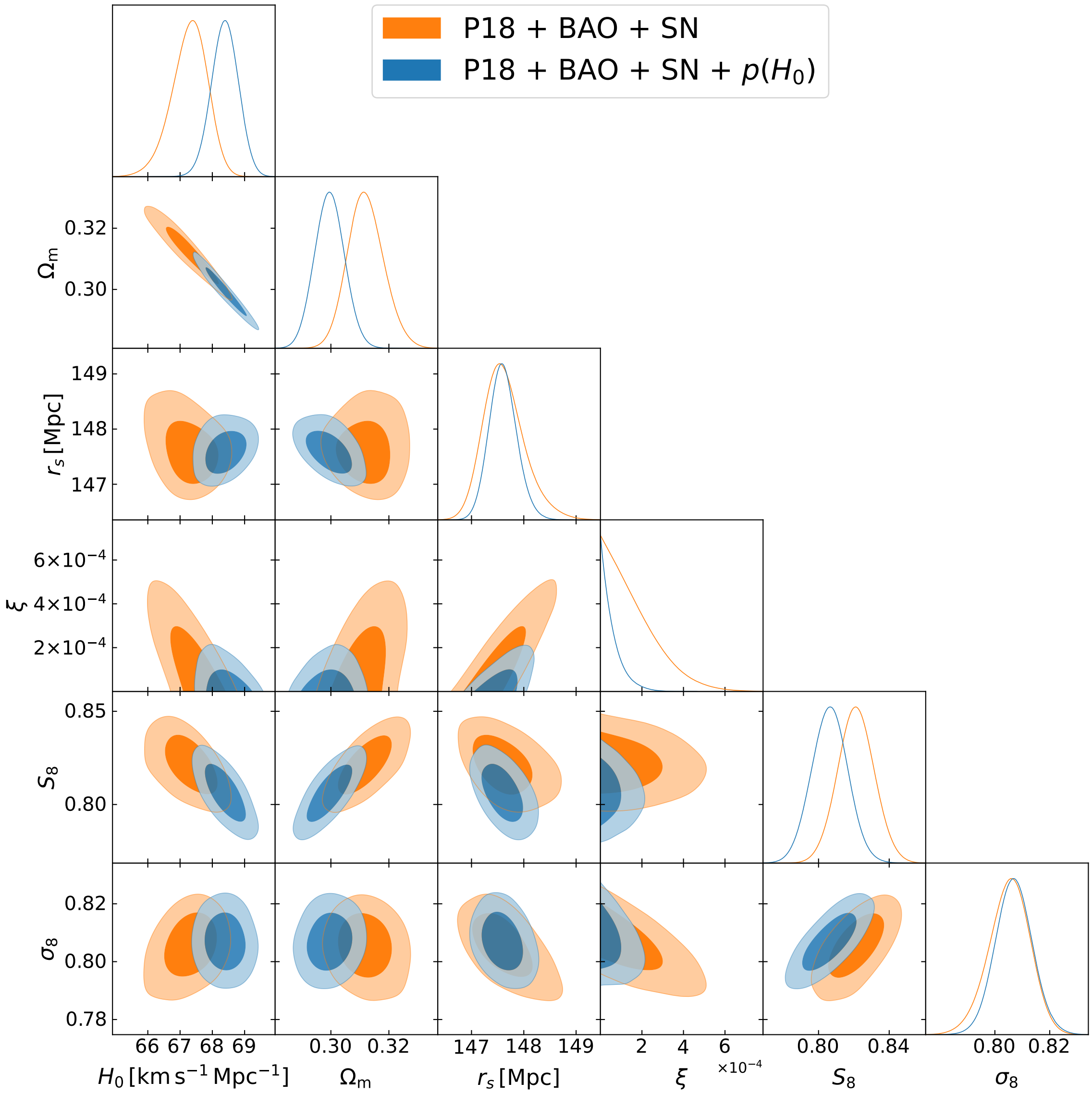

Figure 6. Marginalized joint 68% and 95% C.L. regions 2D parameter space using the combination CMB+BAO+SN (orange) and CMB+BAO+SN+$p(H_0)$ (blue) for IG ($F = \xi\sigma^2$, $V = \lambda F^2/4$) in the phantom branch ($Z = -1$).

containing also a Galileon term G_3 [83, 84] as in $\mathcal{L} = G_4(\sigma)R + G_2(\sigma, X) + G_3(\sigma, X)\Box\sigma$, the conditions for the avoidance of such instabilities are

$$q_s \equiv 4G_4\{G_{2X} + 2G_{3\sigma} + \dot\sigma[(G_{2XX} + G_{3X\sigma})\dot\sigma - 6G_{3X}H]\} + 3(2G_{4\sigma} + G_{3X}\dot\sigma^2)^2 > 0 \quad (3.13)$$

$$\begin{aligned} c_s^2 \equiv\ & [4G_{2X}G_4 + 8G_{3\sigma}G_4 + (6G_{4\sigma}^2 - G_{3X}\dot\sigma^2)(2G_{4\sigma}^2 + G_{3X}\dot\sigma^2) \\ & - 8G_4(G_{3X}\ddot\sigma + 2G_{3X}H\dot\sigma + G_{3X\sigma}\dot\sigma^2)]/q_s > 0, \end{aligned} \quad (3.14)$$

which reduce to eqs. (2.8), (2.9) when $G_3 = 0$; but, in general, depending on the functional form of the cubic interaction term and its magnitude, can allow for $\xi < 1/6$ while maintaining the theory free of ghost and Laplacian instabilities [77, 85–87].

3.2 Phantom non-minimal coupling

For NMC+ (NMC-) [14], with coupling $F(\sigma) = N_{\rm Pl}^2 + \xi\sigma^2$ and coupling $V(\sigma) = \lambda F^2(\sigma)/4$, we sample on the dimensionless parameter $\Delta\tilde{N}_{\rm Pl} \equiv N_{\rm Pl}/M_{\rm Pl} - 1$ and ξ.

We show the results for all the combinations of datasets on figure 7 for NMC+ and for NMC- in figure 8. Marginalized constraints on cosmological parameters are consistent to the results obtained for IG for each combination of datasets. The marginalized limits on the coupling parameters for NMC+ (NMC-) at 95% C.L. correspond to $\xi < 0.0015$ (> -0.039) and $N_{\rm Pl} > 0.91$ (< 1.18) for P18+BAO, and to $\xi < 0.0019$ (> -0.027) and $N_{\rm Pl} > 0.83$ (< 1.21) for P18+BAO+SN; see tables 2 and 3 for the constraints on all the parameters. As observed in refs. [14, 19], there is a strong degeneracy between the coupling parameters $N_{\rm Pl}$ and ξ for the form of non-minimal coupling $F(\sigma) = N_{\rm Pl}^2 + \xi\sigma^2$. Since cosmological observables are affected by contributions $\mathcal{O}\left(\xi\sigma^2/N_{\rm Pl}^2\right)$, it is possible to compensate the effects due to a large value of $|\xi|$ increasing $|\tilde{N}_{\rm Pl} - 1|$ and vice versa.

In this case eqs. (2.8), (2.9) reduce to

$$\left(\frac{N_{\rm Pl}}{\xi\sigma}\right)^2 + \frac{1}{\xi} < 6\,. \tag{3.15}$$

Also in this case, a large portion of the allowed parameter space is at odds with eq. (3.15) despite the larger number of degrees of freedom.

3.3 Phantom early modified gravity

For EMG [20], with coupling $F(\sigma) = M_{\rm Pl}^2 + \xi\sigma^2$ and potential $V(\sigma) = \Lambda + \lambda\sigma^4/4$, we sample on the quantity ξ and V_0 where $\lambda \equiv -10^{2V_0}/M_{\rm Pl}^4$. The scalar field decays around the local maximum of the potential, i.e. $\sigma = 0$, showing tachyon instability. In this case, we do not have to impose the boundary condition (3.1) being automatically satisfied for each initial value of scalar field. This leads to a third free parameter which we identify with the initial value of the scalar field $\sigma_{\rm ini}$ $[M_{\rm Pl}]$.

In figure 9, we compare the background evolution and spectra of EMG in the standard branch ($Z = 1$) to the phantom branch case ($Z = -1$). The evolution of the scalar field σ is very similar in the two cases. Starting with the scalar field at rest in the radiation era, it starts to grow around the recombination driven by the coupling to the non-relativistic matter component and it is subsequently driven into damped coherent oscillations from the quartic potential. The different evolution of the coupling function, which increase in the branch with standard kinetic term while decreasing in the phantom branch before the scalar field starts to decay, due to the different sign of the coupling parameter ξ induces different effects on the spectra. The acoustic peaks of the CMB temperature anisotropies angular power spectrum are shifted to right in the standard branch ($Z = 1$) when the scalar field starts to move before recombination ($V_0 = 2$) and in the phantom branch ($Z = -1$) if the scalar field decays after recombination ($V_0 = -1$), vice versa they shift to the left with respect the ΛCDM case. The situation is different on the linear matter power spectrum were we observe a suppression of power in the standard branch ($Z = 1$) despite the value of V_0 and an increase of power at small scales in the phantom branch ($Z = -1$). This highlights the importance of the combination of combining early- and late-time probes in order to break the degeneracy between the extra parameters of the model and also to discriminate between the two different branches.

We show the results for the combinations of datasets P18+BAO+SN and P18+BAO+SN+$p(H_0)$ on figure 10. In this case we find that ξ is not constrained by data on the

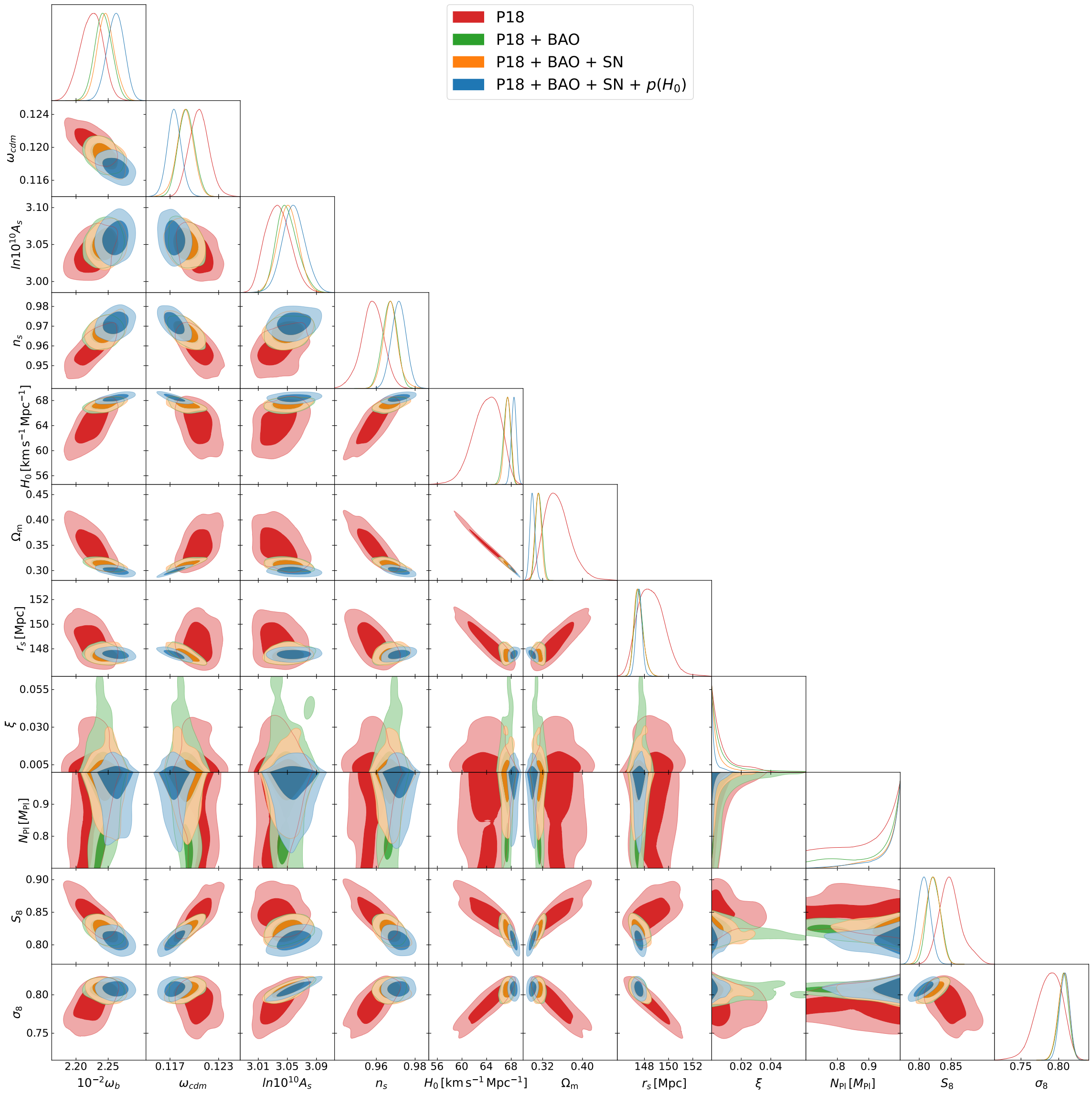

Figure 7. Marginalized joint 68% and 95% C.L. regions 2D parameter space using the P18 (green), the combination P18+BAO (orange), and the combination P18+BAO+SN (blue) for NMC+ ($F = N_{\rm Pl}^2 + \xi\sigma^2$, $V = \lambda F^2/4$) in the phantom branch ($Z = -1$).

prior considered $[-0.1, 0]$. For this reason, we show constraints on the combination $\xi\sigma_{\rm ini}^2$ $[M_{\rm Pl}^2]$ (connected to the additional contribution to the expansion rate evolution (3.2) before recombination). The marginalized upper bound on the coupling combination $\xi\sigma_{\rm ini}^2$ at 95% C.L. corresponds to > -0.0026 for P18+BAO+SN and when we include the Gaussian prior on the Hubble parameter we obtain at 95% C.L. -0.006 ± 0.005. Analogously, for the initial value of the scalar field $\sigma_{\rm ini}$ $[M_{\rm Pl}]$ we find < 0.45 for P18+BAO+SN and $0.35^{+0.17}_{-0.15}$ for P18+BAO+SN+$p(H_0)$ both at 95% C.L. Also V_0 is not well constrained. We find a 95% C.L. upper bound only when we include the Gaussian prior on the Hubble parameter corresponding to $V_0 < 0.81$.

The marginalized means and uncertainties for the Hubble constant H_0 $\left[\mathrm{km\,s^{-1}\,Mpc^{-1}}\right]$ at 68% C.L. correspond to $68.44^{+0.62}_{-0.79}$ for P18+BAO+SN and $70.18^{+0.59}_{-0.68}$ for P18+BAO+SN

JCAP04(2023)029

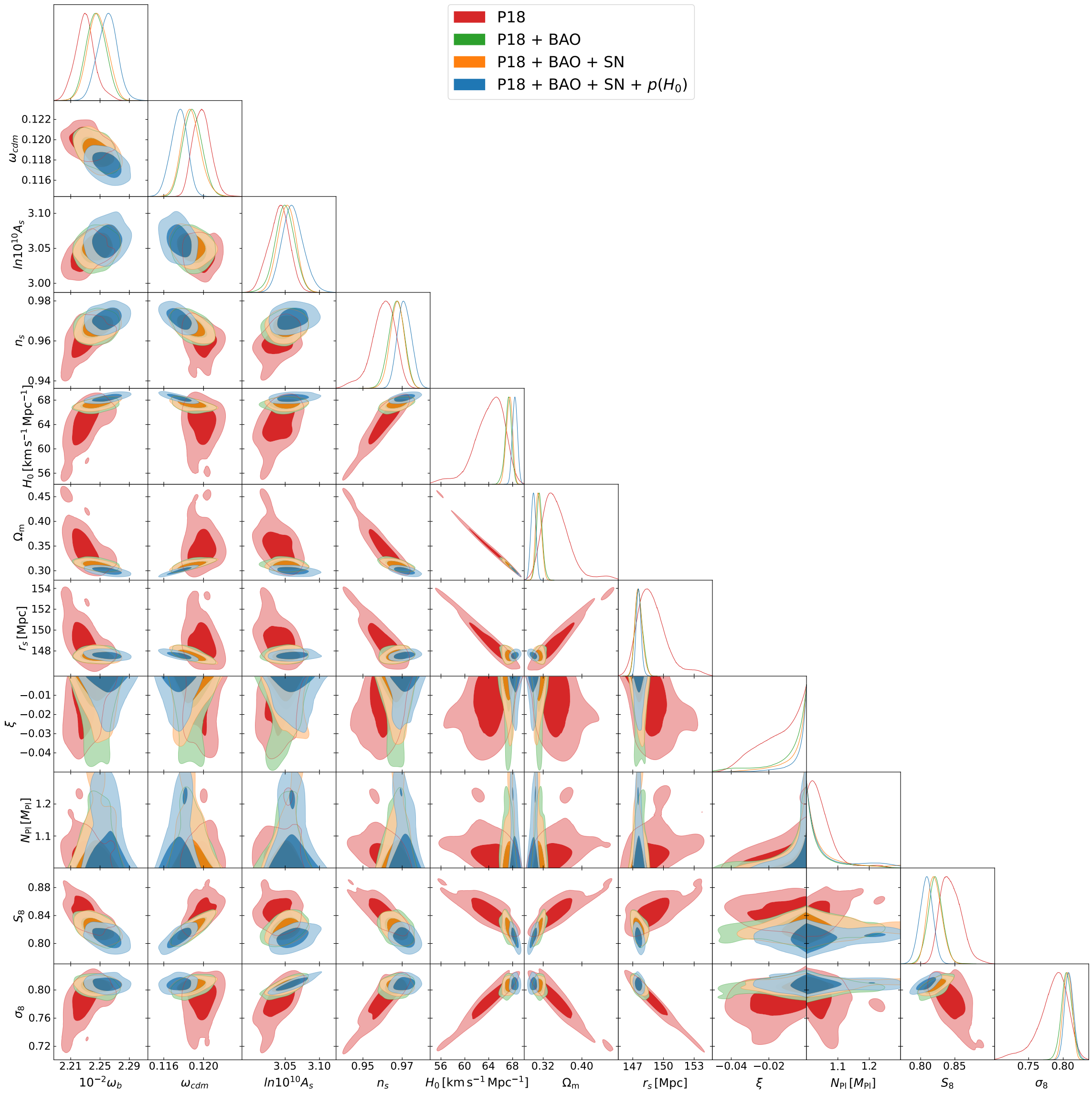

Figure 8. Marginalized joint 68% and 95% C.L. regions 2D parameter space using the P18 (red), the combination P18+BAO (green), the combination P18+BAO+SN (orange), and the combination P18+BAO+SN+$p(H_0)$ (blue) for NMC- ($F = N_{\rm Pl}^2 + \xi\sigma^2$, $V = \lambda F^2/4$) in the phantom branch ($Z = -1$).

$+p(H_0)$. The marginalized constraints on S_8 correspond to $S_8 = 0.827 \pm 0.011$ for P18+BAO+SN and $S_8 = 0.822 \pm 0.010$ for P18+BAO+SN+$p(H_0)$. See table 5 for the constraints on all the parameters. Finally, we show in table 6 the best-fit $\Delta\chi^2$ for all the four model analyzed with respect to the ΛCDM model for each dataset for the combination P18+BAO+SN and P18+BAO+SN+$p(H_0)$.

4 Conclusions

We have studied the dynamics and inferred the cosmological constraints for modified gravity models with a nonminimally coupled scalar with a kinetic term which can also have a negative

JCAP04(2023)029

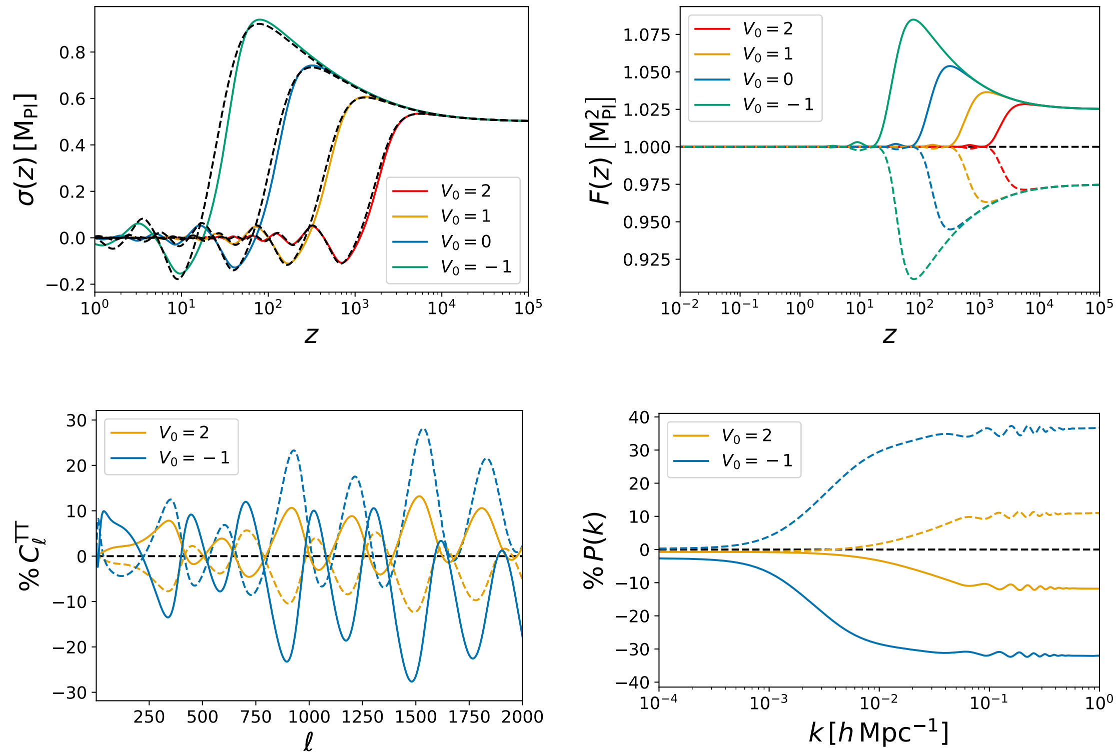

Figure 9. Time evolution of the scalar field σ (upper left panel) and of the coupling to the Ricci scalar $F(\sigma)$ (upper right panel). Relative differences of the CMB temperature anisotropies power spectrum with respect to the ΛCDM case (bottom left panel) and of the linear matter power spectrum at $z = 0$ (bottom right panel). Different lines correspond to different value of the amplitude of the effective potential V_0 for $|\xi| = 0.1$ in the standard branch (solid lines) and in the phantom one (dashed lines) for EMG ($F = M_{\rm Pl}^2 + \xi\sigma^2$, $V = \Lambda + \lambda\sigma^4/4$).

sign. For stable models with an effectively massless scalar field σ, like IG and NMC, the change of sign in front of the kinetic term of the scalar field modifies the evolution of the scalar field which is at rest during the radiation-dominated epoch and evolves like $\sigma \sim a^{2Z\xi}$ during the matter-dominated era.

We have shown the effect of the sign of the kinetic term on cosmological observables. We have computed the marginalized constraints for different combination of cosmological datasets by allowing the coupling to the Ricci scalar and the rest of cosmology (standard cosmological parameters and nuisance ones) to vary. Combining *Planck* 2018 DR3 measurements with BAO from BOSS and eBOSS, and uncalibrated SN Iα from the Pantheon sample we constrain the coupling parameters at 95% C.L. to $\xi < 0.00040$ for $F(\sigma) = \xi\sigma^2$ and for $F(\sigma) = N_{\rm Pl}^2 + \xi\sigma^2$ to $\xi < 0.0019$ (> -0.027) and $N_{\rm Pl} > 0.83$ (< 1.21).

Nonminimally coupled scalar-tensor theories with early-time deviation from GR predictions usually lead to higher values of the Hubble parameter H_0, a lower value of the matter density parameter $\Omega_{\rm m}$, and a larger value of the σ_8 [19, 77, 78]. In their phantom construction, the modified evolution of the scalar field, connected to a different time evolution of the effective gravitational constant, inverts the degeneracy between these parameters and the coupling ones. Indeed, we find a lower values of both σ_8 and H_0 compared to the branch with standard kinetic term.

JCAP04(2023)029

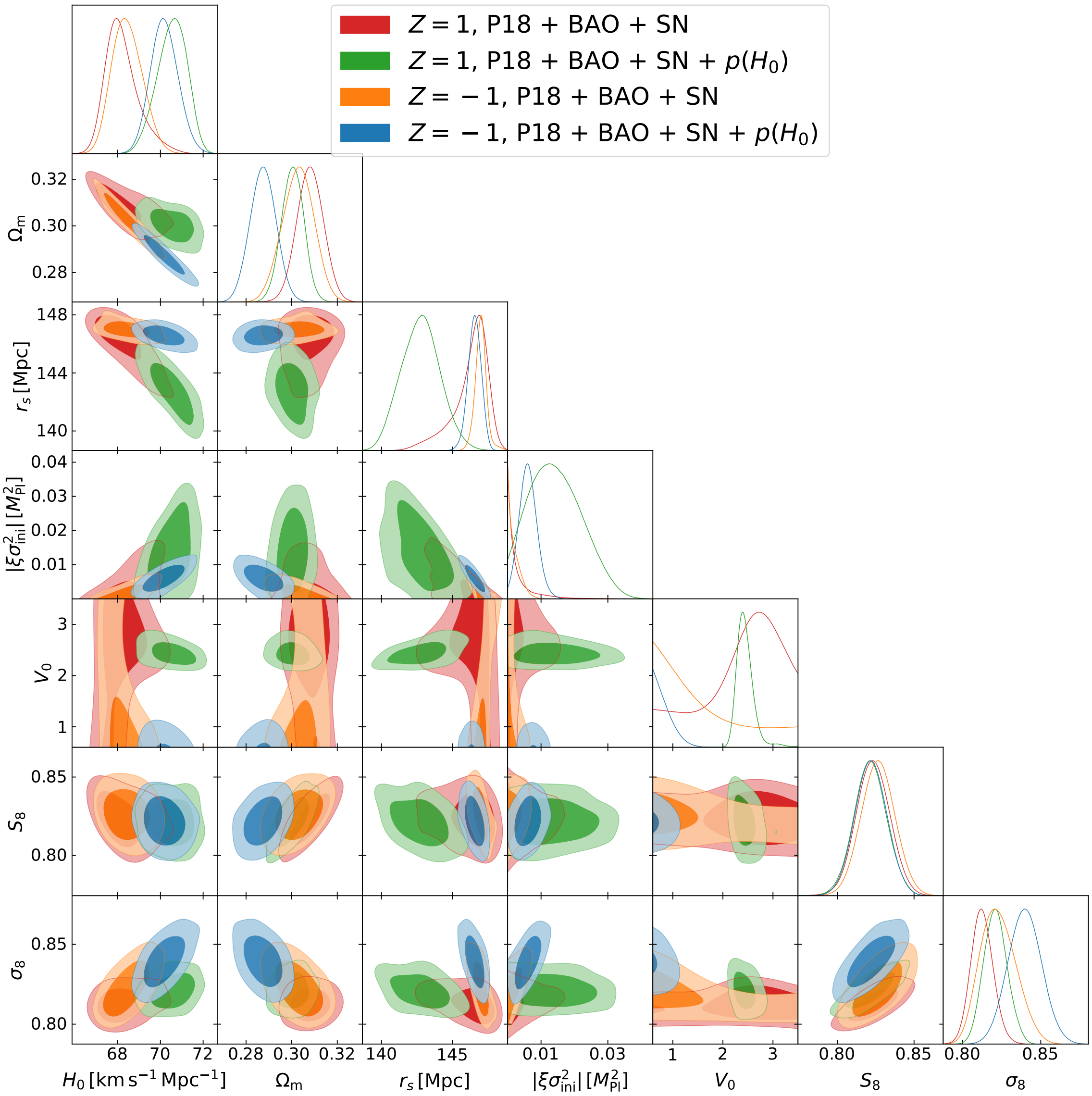

Figure 10. Marginalized joint 68% and 95% C.L. regions 2D parameter space using P18+BAO+SN (orange) and the combination P18+BAO+SN+$p(H_0)$ (blue) for EMG ($F = M^2_{\rm Pl}+\xi\sigma^2$, $V = \Lambda+\lambda\sigma^4/4$) in the phantom branch ($Z = -1$).

We have also studied the phantom version of the EMG model introduced in ref. [20]. While the evolution of the scalar field is very similar, with the quartic potential leading the scalar field to decay into damped coherent oscillations, different signatures appear on the cosmological observables. Compared to the ΛCDM model, the CMB acoustic peaks of the CMB are shifted to right in the standard branch ($Z = 1$) when the scalar field starts to move before recombination ($V_0 = 2$) and in the phantom branch ($Z = -1$) if the scalar field decays after recombination ($V_0 = -1$), vice versa they shift to the left. Matter perturbations on sub-horizon scales are suppressed in the standard branch ($Z = 1$) and enhanced in the phantom branch ($Z = -1$) despite the value of amplitude of the self-interaction term parameterized by V_0.

JCAP04(2023)029

The allowed parameter space for the coupling parameters by our analysis is at odds with the parameter space free from ghosts and Laplacian instabilities. It would be interesting to understand if instead there are healthy scalar-tensor theories which retain the possibility to alleviate the current tensions between different cosmological observations.

Acknowledgments

MB and FF acknowledge financial support from the INFN InDark initiative and from the COSMOS network (www.cosmosnet.it) through the ASI (Italian Space Agency) Grants 2016-24-H.0 and 2016-24-H.1-2018, as well as 2020-9-HH.0 (participation in LiteBIRD phase A). This work has made use of computational resources of INAF OAS Bologna and of the CNAF HPC cluster in Bologna.

A Tables

	P18	P18 + BAO	P18 + BAO + SN
ω_b	0.02223 ± 0.00017	0.02244 ± 0.00013	0.02245 ± 0.00013
ω_c	0.1204 ± 0.0012	0.11896 ± 0.00099	0.11882 ± 0.00096
H_0 [$\mathrm{km\,s^{-1}\,Mpc^{-1}}$]	$63.6^{+2.7}_{-1.9}$	$67.17^{+0.65}_{-0.48}$	$67.29^{+0.60}_{-0.47}$
τ	0.0523 ± 0.0071	$0.0584^{+0.0070}_{-0.0083}$	$0.0584^{+0.0068}_{-0.0076}$
$\ln(10^{10} A_\mathrm{s})$	3.037 ± 0.015	$3.051^{+0.014}_{-0.016}$	3.051 ± 0.014
n_s	$0.9574^{+0.0067}_{-0.0057}$	0.9668 ± 0.0038	0.9671 ± 0.0036
ξ	< 0.0018 (95% C.L.)	< 0.00046 (95% C.L.)	< 0.00040 (95% C.L.)
γ_PN	> 0.9928 (95% C.L.)	> 0.9982 (95% C.L.)	> 0.9984 (95% C.L.)
$\delta G_\mathrm{N}/G_\mathrm{N}$ $(z=0)$	< 0.057 (95% C.L.)	< 0.014 (95% C.L.)	< 0.012 (95% C.L.)
$10^{13}\dot{G}_\mathrm{N}/G_\mathrm{N}$ $(z=0)$ [yr^{-1}]	< 2.43 (95% C.L.)	< 0.57 (95% C.L.)	< 0.50 (95% C.L.)
G_N/G $(z=0)$	$0.9982^{+0.0013}_{-0.00074}$	$0.99965^{+0.00033}_{-0.00013}$	$0.99968^{+0.00030}_{-0.00012}$
Ω_m	$0.354^{+0.020}_{-0.032}$	$0.3135^{+0.0059}_{-0.0068}$	$0.3120^{+0.0056}_{-0.0065}$
σ_8	$0.784^{+0.021}_{-0.015}$	$0.8053^{+0.0083}_{-0.0069}$	$0.8053^{+0.0078}_{-0.0066}$
S_8	$0.850^{+0.016}_{-0.019}$	0.823 ± 0.011	0.821 ± 0.010
r_s [Mpc]	$148.89^{+0.8}_{-1.4}$	$147.62^{+0.31}_{-0.50}$	$147.62^{+0.29}_{-0.44}$
$\Delta\chi^2$	-2.8	0	-0.5

Table 1. Constraints on the main and derived parameters (at 68% C.L. if not otherwise stated) considering P18 in combination with BAO and BAO+SN for the *IG* model.

	P18	P18 + BAO	P18 + BAO + SN
ω_b	$0.02224^{+0.00018}_{-0.00016}$	0.02246 ± 0.00013	$0.02246^{+0.00011}_{-0.00014}$
ω_c	0.1206 ± 0.0012	$0.1190^{+0.0014}_{-0.0011}$	0.1189 ± 0.0010
H_0 [$\mathrm{km\,s^{-1}\,Mpc^{-1}}$]	$64.1^{+2.6}_{-1.7}$	67.28 ± 0.59	67.42 ± 0.52
τ	0.0514 ± 0.0081	0.0590 ± 0.0052	0.0583 ± 0.0071
$\ln(10^{10} A_\mathrm{s})$	$3.037^{+0.015}_{-0.023}$	$3.0517^{+0.0074}_{-0.015}$	3.051 ± 0.014
n_s	$0.9580^{+0.0058}_{-0.0047}$	0.9673 ± 0.0042	0.9674 ± 0.0039
ξ	< 0.030 (95% C.L.)	< 0.015 (95% C.L.)	< 0.019 (95% C.L.)
N_Pl [M_Pl]	—	> 0.91 (95% C.L.)	> 0.83 (95% C.L.)
γ_PN	> 0.9941 (95% C.L.)	> 0.9986 (95% C.L.)	> 0.9987 (95% C.L.)
β_PN	> 0.999965 (95% C.L.)	> 0.999994 (95% C.L.)	> 0.999994 (95% C.L.)
$\delta G_\mathrm{N}/G_\mathrm{N}$ $(z=0)$	< 0.052 (95% C.L.)	< 0.011 (95% C.L.)	< 0.012 (95% C.L.)
$10^{13}\dot{G}_\mathrm{N}/G_\mathrm{N}$ $(z=0)$ [$\mathrm{yr^{-1}}$]	< 1.94 (95% C.L.)	< 0.42 (95% C.L.)	< 0.40 (95% C.L.)
G_N/G $(z=0)$	$1.00134^{+0.00063}_{-0.0011}$	$1.000255^{+0.000097}_{-0.00024}$	$1.000221^{+0.000084}_{-0.00023}$
Ω_m	$0.349^{+0.017}_{-0.030}$	$0.3121^{+0.0068}_{-0.0056}$	0.3110 ± 0.0061
σ_8	$0.788^{+0.021}_{-0.013}$	0.8069 ± 0.0069	$0.8064^{+0.0079}_{-0.0065}$
S_8	$0.849^{+0.013}_{-0.019}$	$0.823^{+0.014}_{-0.009}$	$0.821^{+0.012}_{-0.011}$
r_s [Mpc]	$148.56^{+0.90}_{-1.3}$	$147.54^{+0.30}_{-0.48}$	$147.52^{+0.27}_{-0.44}$
$\Delta\chi^2$	-1.5	0	-0.5

Table 2. Constraints on the main and derived parameters (at 68% C.L. if not otherwise stated) considering P18 in combination with BAO and BAO+SN for the *NMC+* model.

JCAP04(2023)029

	P18	P18 + BAO	P18 + BAO + SN
$\omega_{\rm b}$	0.02230 ± 0.00014	0.02245 ± 0.00013	0.02247 ± 0.00013
$\omega_{\rm c}$	$0.11982^{+0.00068}_{-0.0011}$	0.11891 ± 0.00094	$0.11875^{+0.00078}_{-0.0010}$
H_0 [km s^{-1} Mpc^{-1}]	$64.1^{+3.1}_{-2.1}$	$67.26^{+0.59}_{-0.45}$	$67.44^{+0.57}_{-0.45}$
τ	$0.0548^{+0.0072}_{-0.0059}$	$0.0573^{+0.0061}_{-0.0074}$	0.0590 ± 0.0068
$\ln\left(10^{10} A_{\rm s}\right)$	$3.041^{+0.017}_{-0.013}$	3.049 ± 0.014	$3.052^{+0.014}_{-0.012}$
$n_{\rm s}$	$0.9604^{+0.0067}_{-0.0045}$	$0.9669^{+0.0043}_{-0.0035}$	0.9675 ± 0.0036
ξ	> -0.036 (95% C.L.)	> -0.039 (95% C.L.)	> -0.027 (95% C.L.)
$N_{\rm Pl}$ [$M_{\rm Pl}$]	< 1.13 (95% C.L.)	< 1.18 (95% C.L.)	< 1.21 (95% C.L.)
$\gamma_{\rm PN}$	> 0.988 (95% C.L.)	> 0.998 (95% C.L.)	> 0.998 (95% C.L.)
$\beta_{\rm PN}$	< 1.00018 (95% C.L.)	< 1.000022 (95% C.L.)	< 1.000017 (95% C.L.)
$\delta G_{\rm N}/G_{\rm N}$ $(z=0)$	< 0.060 (95% C.L.)	< 0.012 (95% C.L.)	< 0.010 (95% C.L.)
$10^{13}\dot{G}_{\rm N}/G_{\rm N}$ $(z=0)$ [yr^{-1}]	< 3.85 (95% C.L.)	< 0.62 (95% C.L.)	< 0.50 (95% C.L.)
$G_{\rm N}/G$ $(z=0)$	$1.00224^{+0.00080}_{-0.0021}$	$1.00037^{+0.00012}_{-0.00037}$	$1.00030^{+0.00012}_{-0.00030}$
$\Omega_{\rm m}$	$0.348^{+0.021}_{-0.033}$	$0.3125^{+0.0052}_{-0.0065}$	$0.3106^{+0.0050}_{-0.0068}$
σ_8	$0.786^{+0.025}_{-0.011}$	0.8047 ± 0.0076	0.8064 ± 0.0062
S_8	$0.844^{+0.011}_{-0.018}$	0.821 ± 0.011	$0.8204^{+0.0091}_{-0.012}$
r_s [Mpc]	$148.91^{+0.77}_{-1.6}$	$147.60^{+0.28}_{-0.43}$	$147.57^{+0.30}_{-0.40}$
$\Delta\chi^2$	-2.8	0	-0.3

Table 3. Constraints on the main and derived parameters (at 68% C.L. if not otherwise stated) considering P18 in combination with BAO and BAO+SN for the *NMC*- model.

JCAP04(2023)029

	IG	NMC+	NMC-
$\omega_{\rm b}$	$0.02260^{+0.00012}_{-0.00014}$	0.02262 ± 0.00013	$0.02260^{+0.00014}_{-0.00012}$
$\omega_{\rm c}$	0.11747 ± 0.00086	0.11752 ± 0.00086	$0.11753^{+0.00095}_{-0.00069}$
H_0 [km s^{-1} Mpc^{-1}]	68.34 ± 0.41	$68.42^{+0.44}_{-0.36}$	68.38 ± 0.41
τ	$0.0617^{+0.0067}_{-0.0085}$	$0.0636^{+0.0071}_{-0.0081}$	$0.0644^{+0.0068}_{-0.0090}$
$\ln\left(10^{10} A_{\rm s}\right)$	$3.055^{+0.013}_{-0.017}$	$3.059^{+0.014}_{-0.016}$	$3.061^{+0.014}_{-0.017}$
$n_{\rm s}$	0.9711 ± 0.0036	0.9716 ± 0.0037	0.9712 ± 0.0035
ξ	< 0.000075 (95% C.L.)	< 0.0096 (95% C.L.)	> -0.022 (95% C.L.)
$N_{\rm Pl}$ [$M_{\rm Pl}$]	0	> 0.82 (95% C.L.)	< 1.24 (95% C.L.)
$\gamma_{\rm PN}$	> 0.9993 (95% C.L.)	> 0.9995 (95% C.L.)	> 0.9994 (95% C.L.)
$\beta_{\rm PN}$	1	> 0.999999 (95% C.L.)	< 1.000004 (95% C.L.)
$\delta G_{\rm N}/G_{\rm N}$ $(z=0)$	< 0.0056 (95% C.L.)	< 0.0041 (95% C.L.)	< 0.0042 (95% C.L.)
$10^{13}\dot{G}_{\rm N}/G_{\rm N}$ $(z=0)$ [yr^{-1}]	< 0.23 (95% C.L.)	< 0.16 (95% C.L.)	< 0.19 (95% C.L.)
$G_{\rm N}/G$ $(z=0)$	$0.99987^{+0.00013}_{-0.000042}$	$1.000080^{+0.000028}_{-0.000090}$	$1.000102^{+0.000043}_{-0.00011}$
$\Omega_{\rm m}$	0.2999 ± 0.0050	$0.2994^{+0.0046}_{-0.0052}$	$0.2997^{+0.0053}_{-0.0047}$
σ_8	$0.8055^{+0.0059}_{-0.0069}$	0.8078 ± 0.0066	0.8086 ± 0.0063
S_8	0.805 ± 0.010	0.807 ± 0.010	0.8082 ± 0.0094
r_s [Mpc]	$147.63^{+0.23}_{-0.29}$	147.56 ± 0.25	$147.58^{+0.21}_{-0.24}$

Table 4. Constraints on the main and derived parameters (at 68% C.L. if not otherwise stated) considering the combination with P18+BAO+SN+$p(H_0)$ for *IG*, *NMC+*, and *NMC-*.

JCAP04(2023)029

	P18 + BAO + SN	P18 + BAO + SN + $p(H_0)$
$\omega_{\rm b}$	0.02246 ± 0.00014	0.02255 ± 0.00014
$\omega_{\rm c}$	0.1194 ± 0.0010	0.11900 ± 0.00099
H_0 [km s^{-1} Mpc^{-1}]	$68.44^{+0.62}_{-0.79}$	$70.18^{+0.59}_{-0.68}$
τ	0.0536 ± 0.0080	$0.0503^{+0.0085}_{-0.0073}$
$\ln\left(10^{10} A_{\rm s}\right)$	3.043 ± 0.016	$3.035^{+0.017}_{-0.015}$
$n_{\rm s}$	$0.9671^{+0.0036}_{-0.0042}$	0.9687 ± 0.0038
$\xi\sigma^2_{\rm ini}$ [$M^2_{\rm Pl}$]	> -0.0057 (95% C.L.)	$-0.0062^{+0.0028}_{-0.0023}$
V_0	—	< 0.81 (95% C.L.)
$\sigma_{\rm ini}$ [$M_{\rm Pl}$]	< 0.446 (95% C.L.)	$0.348^{+0.062}_{-0.097}$
$\Omega_{\rm m}$	0.3028 ± 0.0068	0.2875 ± 0.0056
σ_8	$0.823^{+0.010}_{-0.013}$	0.840 ± 0.011
S_8	0.827 ± 0.011	0.822 ± 0.010
r_s [Mpc]	147.00 ± 0.40	146.56 ± 0.46

Table 5. Constraints on the main and derived parameters (at 68% C.L. if not otherwise stated) considering P18 in combination with BAO+SN and BAO+SN+$p(H_0)$ for the *EMG* model.

JCAP04(2023)029

P18+BAO+SN	IG	NMC+	NMC−	EMG ($Z=1$)	EMG ($Z=-1$)
Planck high-ℓ TTTEEE	−1.2	−1.3	−1.6	−0.8	−0.6
Planck low-ℓ EE	0.4	0.4	1	0.1	−0.3
Planck low-ℓ TT	0.2	0.3	0.3	−0.2	0.5
Planck lensing	−0.2	−0.2	−0.3	0	0.8
BAO	0.2	0.2	0.2	0	−0.5
Pantheon	0.1	0.1	0.1	0	−0.2
Total	−0.5	−0.5	−0.3	−0.9	−0.3

P18+BAO+SN+$p(H_0)$	IG	NMC+	NMC−	EMG ($Z=1$)	EMG ($Z=-1$)
Planck high-ℓ TTTEEE	−1.2	−0.8	−1.4	−0.7	−6.5
Planck low-ℓ EE	0.8	0.4	0.7	0.4	−1.8
Planck low-ℓ TT	−0.1	−0.2	−0.2	−0.2	1.1
Planck lensing	−0.1	−0.1	−0.2	−0.1	0.6
BAO	0.1	0.1	0	0	5
Pantheon	0	0	0	0	0.4
H_0	0	0.2	0.6	−17.8	−13.7
Total	−0.5	−0.4	−0.5	−18.4	−14.9

Table 6. Best-fit $\Delta\chi^2$ with respect to the ΛCDM model for each dataset for the combination P18+BAO+SN (upper table) and P18+BAO+SN+$p(H_0)$ (lower table) for *IG*, *NMC+*, *NMC-*, and *EMG*.

B Background equations

Starting from eq. (2.1), it is possible to write down the equations governing the background evolution. Specializing to a spatially flat Friedmann-Lemaître-Robertson-Walker (FLRW) universe described by the line element

$$\mathrm{d}s^2 = a^2(\eta)\left(-\mathrm{d}\eta^2 + \mathrm{d}\mathbf{x}^2\right), \tag{B.1}$$

where η is the conformal time and $\mathbf{x}$ the spatial comoving coordinate. The Einstein equations are obtained by varying the action (2.1) with respect to the metric, they correspond to

$$G^{\mu}{}_{\nu} = \frac{1}{F}\left[T^{\mu}_{\ \nu} - \frac{Z}{2}\nabla^{\mu}\sigma\nabla_{\nu}\sigma - g^{\mu}{}_{\nu}V + \left(\nabla^{\mu}\nabla_{\nu} - g^{\mu}{}_{\nu}\Box\right)F\right] \tag{B.2}$$

where the energy-momentum tensor for a perfect fluid is given by

$$T_{\mu\nu} = p g_{\mu\nu} + (\rho + p)u_{\mu}u_{\nu} \tag{B.3}$$

where a sum over all the species in the Universe is taken for granted, i.e. $\rho \equiv \sum_i \rho_i$ and $p \equiv \sum_i p_i$.

From eq. (B.2), the Friedmann equations in Jordan frame are as follows

$$3F\,\mathcal{H}^2 = a^2(\rho + V) + \frac{Z\sigma'^2}{2} - 3\mathcal{H}F' \tag{B.4}$$

$$-2F\,\mathcal{H}' = \frac{a^2}{3}(\rho + 3p - 2V) + \frac{2}{3}Z\sigma'^2 + F'' \tag{B.5}$$

and the Einstein trace (the Ricci scalar) equation results

$$a^2FR = a^2(\rho - 3p) + 4a^2V - 3F_{\sigma}\left(\sigma'' + 2\mathcal{H}\sigma'\right) - (Z + 3F_{\sigma\sigma})\sigma'^2\,. \tag{B.6}$$

Finally, the evolution equation of the scalar field σ is governed by the modified Klein-Gordon equation

$$\sigma'' + 2\mathcal{H}\sigma' - \frac{F_{\sigma}}{2ZF + 3F_{\sigma}^2}\left[a^2(\rho - 3p) + 4a^2\left(V - \frac{F}{2F_{\sigma}}V_{\sigma}\right) - (Z + 3F_{\sigma\sigma})\,\sigma'^2\right] = 0\,. \tag{B.7}$$

C Linear perturbed equations

In the synchronous gauge, up to linear order in perturbed quantities, the perturbed FLRW metric is

$$\mathrm{d}s^2 = a^2(\eta)\left[-\mathrm{d}^2\eta + (\delta_{ij} + h_{ij})\mathrm{d}x^i\mathrm{d}x^j\right] \tag{C.1}$$

where h_{ij} is the metric perturbation.

From this point on, we move in Fourier space for the calculation of the perturbed quantities. The scalar mode of h_{ij} can be express as a Fourier integral as

$$h_{ij}(\eta, \mathbf{x}) = \int \mathrm{d}^3k e^{\imath\mathbf{k}\cdot\mathbf{x}}\left[\hat{k}_i\hat{k}_j h(\eta, \mathbf{k}) + \left(\hat{k}_i\hat{k}_j - \frac{\delta_{ij}}{3}\right)6\xi(\eta, \mathbf{k})\right] \tag{C.2}$$

where $\hat{k}_i = k_i/k$ with $k = |\mathbf{k}|$ and $h \equiv \delta^{ij}h_{ij}$ is the Fourier transform of trace of $h_{ij}(\eta, \mathbf{x})$. We follow the conventions of ref. [88].

JCAP04(2023)029

C.1 The perturbed Einstein field equations

Splitting the Einstein tensor as the sum of the background (mean) part $\bar{G}_{\mu\nu}$ and its corresponding perturbation $\delta G_{\mu\nu}$, i.e. $G_{\mu\nu} = \bar{G}_{\mu\nu} + \delta G_{\mu\nu}$, the scalar perturbations in synchronous gauge are usually presented as time-time, longitudinal time-space, trace space-space, and longitudinal traceless space-space parts of the Einstein equations in Fourier space as follow

$$\begin{aligned}
\xi k^2 - \frac{\mathcal{H}h'}{2} &= a^2 \frac{\delta G^0{}_0}{2} \\
&= 4\pi G a^2 \delta T^0{}_0 \,, && \text{(C.3)} \\
k^2 \xi' &= a^2 \frac{\nabla^i \delta G^0{}_i}{2} \\
&= 4\pi G a^2 (\bar{\rho} + \bar{p})\theta \,, && \text{(C.4)} \\
h'' + 2\mathcal{H}h' - 2\xi k^2 &= -a^2 \delta G^i{}_i \\
&= -8\pi G a^2 \delta T^i{}_i \,, && \text{(C.5)} \\
h'' + 6\xi'' + 2\mathcal{H}(h' + 6\xi') - 2k^2\xi &= -3a^2 \left(\hat{k}_i \hat{k}_j - \frac{\delta_{ij}}{3}\right) \delta G^i{}_i \\
&= -24\pi G a^2 (\bar{\rho} + \bar{p})\Theta && \text{(C.6)}
\end{aligned}$$

where we used the definition

$$\begin{aligned}
(\bar{\rho} + \bar{p})\theta &\equiv \imath k^i \delta T^0{}_i \,, && \text{(C.7)} \\
(\bar{\rho} + \bar{p})\Theta &\equiv -\left(\hat{k}_i \hat{k}_j - \frac{\delta_{ij}}{3}\right) \Sigma^i{}_j \,, && \text{(C.8)} \\
\Sigma^i{}_j &\equiv \bar{T}^i{}_j - \delta^i_j \frac{\bar{T}^k{}_k}{3} \,, && \text{(C.9)}
\end{aligned}$$

and splitting the total energy density and pressure in a background and perturbed parts, we obtain the following elements

$$\begin{aligned}
\bar{T}_{00} &= a^2(\bar{\rho} + \delta\rho) \,, && \text{(C.10)} \\
\bar{T}_{0i} &= -a^2(\bar{\rho} + \bar{p})v^i \,, && \text{(C.11)} \\
\bar{T}_{ij} &= a^2 \delta_{ij} \left(\bar{p} + \delta p\right) + a^2 \Sigma_{ij} \,. && \text{(C.12)}
\end{aligned}$$

The first perturbed equation involving total density fluctuations reads

$$\xi k^2 - \frac{\mathcal{H}h'}{2} = -(8\pi G)a^2 \frac{\delta\tilde{\rho}}{2F} \tag{C.13}$$

with

$$\begin{aligned}
\delta\tilde{\rho} = \delta\rho - \frac{h'\bar{\sigma}'\bar{F}_\sigma}{2a^2} + \frac{\delta\sigma'}{a^2}\left(Z\bar{\sigma}' - 3\mathcal{H}\bar{F}_\sigma\right) - \frac{\delta\sigma \bar{F}_\sigma}{a^2\bar{F}}\Bigg[a^2\bar{\rho} + \frac{Z}{2}\bar{\sigma}'^2 \\
+ a^2\left(V - V_\sigma \frac{F}{F_\sigma}\right) - 3\mathcal{H}\bar{F}_\sigma\bar{\sigma}' + 3\mathcal{H}\frac{F_{\sigma\sigma}F}{F_\sigma}\bar{\sigma}' + k^2 F\Bigg] \,. && \text{(C.14)}
\end{aligned}$$

The second perturbed equation involving total velocity reads

$$k^2\xi' = (8\pi G)a^2\frac{(\tilde\rho+\tilde p)\tilde\theta}{2F} \tag{C.15}$$

with

$$(\tilde\rho+\tilde p)\,\tilde\theta = (\bar\rho+\bar p)\,\theta + \frac{k^2}{a^2}\left[\left(Z\bar\sigma' - \mathcal{H}F_\sigma + F_{\sigma\sigma}\bar\sigma'\right)\delta\sigma + F_\sigma\delta\sigma'\right]. \tag{C.16}$$

The third perturbed equation involving total pressure reads

$$h'' + 2\mathcal{H}h' - 2k^2\xi = -3(8\pi G)a^2\frac{\delta\tilde p}{F} \tag{C.17}$$

with

$$\begin{aligned}\delta\tilde p = \delta p &+ \frac{h'F'}{3a^2} + \frac{Z}{a^2}\bar\sigma'\delta\sigma' - \delta V + \frac{2}{3a^2}k^2\delta F + \frac{\mathcal{H}}{a^2}\delta F' + \frac{\delta F''}{a^2}\\ &- \delta\sigma\frac{\bar F_\sigma}{a^2\bar F}\left(a^2\bar p + \frac{Z}{2}\bar\sigma'^2 - a^2\bar V + \mathcal{H}F' + F''\right).\end{aligned} \tag{C.18}$$

The fourth perturbed equation involving total shear reads

$$h'' + 6\xi'' + 2\mathcal{H}(h' + 6\xi') - 2k^2\xi = -3(8\pi G)a^2\frac{(\tilde\rho+\tilde p)\tilde\Theta}{F} \tag{C.19}$$

with

$$(\tilde\rho+\tilde p)\tilde\Theta = (\bar\rho+\bar p)\Theta + \frac{2k^2}{3a^2}\left(F_\sigma\delta\sigma + F'\frac{h'+6\xi'}{2k^2}\right). \tag{C.20}$$

The perturbed Ricci scalar is given by

$$\begin{aligned}a^2F\delta R = a^2(\delta\bar\rho - 3\delta\bar p) &- \frac{3h'F'}{2} - 2Z\bar\sigma'\delta\sigma' + 4a^2V_\sigma\delta\sigma - 6\mathcal{H}\delta F' - 3\delta F''\\ - 3k^2\delta F &- \frac{\delta\sigma F_\sigma}{F}\left[a^2(\bar\rho - 3\bar p) - Z\bar\sigma'^2 + 4a^2\bar V - 3F'' - 6\mathcal{H}F'\right].\end{aligned} \tag{C.21}$$

C.2 The perturbed Klein-Gordon equation

The perturbed equation for the evolution of the scalar field perturbation $\delta\sigma$ is

$$Z\delta\sigma'' + 2\mathcal{H}Z\delta\sigma' + \left[Zk^2 + a^2\left(V_{\sigma\sigma} - \frac{RF_{\sigma\sigma}}{2}\right)\right]\delta\sigma + Z\frac{h'\bar\sigma'}{2} - \frac{a^2F_\sigma}{2}\delta R = 0. \tag{C.22}$$

D Initial conditions

The adiabatic initial condition for the background correspond to

$$\begin{aligned}a(\tau) &= \sqrt{\frac{\rho_{\mathrm{r}\,0}}{3F_{\mathrm{ini}}}}\tau\left[1 + \frac{Z}{4}\omega\tau - \frac{5ZF_{\mathrm{ini},\sigma}^2\left(Z + 3F_{\mathrm{ini},\sigma\sigma}\right)}{64ZF_{\mathrm{ini}} + 96F_{\mathrm{ini},\sigma}^2}(\omega\tau)^2\right],\\ \mathcal{H}(\tau) &= \frac{1}{\tau}\left[1 + \frac{Z}{4}\omega\tau - Z\frac{2F_{\mathrm{ini}} + F_{\mathrm{ini},\sigma}^2\left(8Z + 15F_{\mathrm{ini},\sigma\sigma}\right)}{32ZF_{\mathrm{ini}} + 48F_{\mathrm{ini},\sigma}^2}(\omega\tau)^2\right],\\ \sigma(\tau) &= \sigma_{\mathrm{ini}} + \frac{3F_{\mathrm{ini},\sigma}}{4}\omega\tau - F_{\mathrm{ini},\sigma}\frac{4ZF_{\mathrm{ini}}(2Z - 3F_{\mathrm{ini},\sigma\sigma}) + 27F_{\mathrm{ini},\sigma}^2\left(Z + F_{\mathrm{ini},\sigma\sigma}\right)}{32(2ZF_{\mathrm{ini}} + 3F_{\mathrm{ini},\sigma}^2)}(\omega\tau)^2\end{aligned} \tag{D.1}$$

where

$$\omega = \frac{\rho_{\mathrm{m},0}}{\sqrt{3\rho_{\mathrm{r},0}}} \frac{2\sqrt{F_{\mathrm{ini}}}}{2ZF_{\mathrm{ini}} + 3F_{\mathrm{ini},\sigma}^2} \,. \tag{D.2}$$

For the cosmological fluctuations in the synchronous gauge, we have as adiabatic initial conditions

$$\delta_\gamma(k\,,\tau) = \delta_\nu(k\,,\tau) = \frac{4}{3}\delta_{\mathrm{b}}(k\,,\tau) = \frac{4}{3}\delta_{\mathrm{c}}(k\,,\tau) = -\frac{(k\tau)^2}{3}\left(1 - \frac{Z\omega\tau}{5}\right) \tag{D.3}$$

$$\theta_\nu(k\,,\tau) = -\frac{k^4\tau^3}{36}\frac{23+4R_\nu}{15+4R_\nu}\left[1 - \frac{3}{20}\frac{Z\left(275+50R_\nu+8R_\nu^2\right)F_{\mathrm{ini}} + 15(5-4R_\nu)F_{\mathrm{ini},\sigma}^2}{(15+2R_\nu)(23+4R_\nu)F_{\mathrm{ini}}}\omega\tau\right] \tag{D.4}$$

$$\theta_\gamma(k\,,\tau) = \theta_{\mathrm{b}}(k\,,\tau) = -\frac{k^4\tau^3}{36}\left[1 - \frac{3}{20}\frac{Z(1-R_\nu+5R_{\mathrm{b}})F_{\mathrm{ini}} + \frac{15}{2}R_{\mathrm{b}}F_{\mathrm{ini},\sigma}^2}{(1-R_\nu)\,F_{\mathrm{ini}}}\omega\tau\right] \tag{D.5}$$

$$\theta_{\mathrm{c}}(k\,,\tau) = 0 \tag{D.6}$$

$$\sigma_\nu(k\,,\tau) = \frac{2(k\tau)^2}{3(15+4R_\nu)}\left[1 + \frac{(-5+4R_\nu)\left(2ZF_{\mathrm{ini}}+3F_{\mathrm{ini},\sigma}^2\right)}{8(15+2R_\nu)F_{\mathrm{ini}}}\omega\tau\right] \tag{D.7}$$

$$h(k\,,\tau) = \frac{(k\tau)^2}{2}\left(1 - \frac{Z\omega\tau}{5}\right) \tag{D.8}$$

$$\eta(k\,,\tau) = 1 - \frac{(k\tau)^2}{12(15+4R_\nu)}\left[5+4R_\nu - \frac{2Z(5+4R_\nu)(65+4R_\nu)F_{\mathrm{ini}} + 75(-5+4R_\nu)F_{\mathrm{ini},\sigma}^2}{20(15+2R_\nu)F_{\mathrm{ini}}}\omega\tau\right] \tag{D.9}$$

$$\delta\sigma(k\,,\tau) = -\frac{1}{16}F_{\mathrm{ini},\sigma}k^2\tau^3\omega\left[1 - \frac{2Z(8Z-9F_{\mathrm{ini},\sigma\sigma})F_{\mathrm{ini}} + (45F_{\mathrm{ini},\sigma\sigma}+48Z)F_{\mathrm{ini},\sigma}^2}{40ZF_{\mathrm{ini}}+60F_{\mathrm{ini},\sigma}^2}\omega\tau\right] \tag{D.10}$$

where $R_\nu = \rho_{\nu,0}/\rho_{\mathrm{r},0}$ and $R_{\mathrm{b}} = \rho_{\mathrm{b},0}/\rho_{\mathrm{m},0}$. These quantities reduce to induced gravity for $Z = 1$ and $F = \xi\sigma^2$ [89], to a non-minimally coupled scalar field with standard kinetic term for $Z = 1$ and $F = N_{\mathrm{Pl}}^2 + \xi\sigma^2$ [14], and General Relativity for $Z = 1$ and $F = M_{\mathrm{Pl}}^2$ [88].

E Comparison between BAO, and FS + BAO joint analysis

We compare here the results adding different datasets of galaxy information to the *Planck* DR3 data such as the full shape (FS) of BOSS DR12 pre-reconstructed power spectrum measurements [66, 67], BAO of BOSS DR12 post-reconstruction power spectrum measurements [68], low-z BAO measurements from SDSS DR7 6dF and MGS [69, 70], Lyα BAO measurements from eBOSS [71–73], and combination of those including the covariance among the DR12 datasets.

In figure 11, we show the marginalized posterior distributions of the cosmological parameters for IG with P18 plus different combinations of the FS and BAO measurements. We see that the posterior distributions are very robust among the combination considered and that the addition of FS information to the combination P18+BAO does not change the marginalized constraints for the models studied here.

JCAP04(2023)029

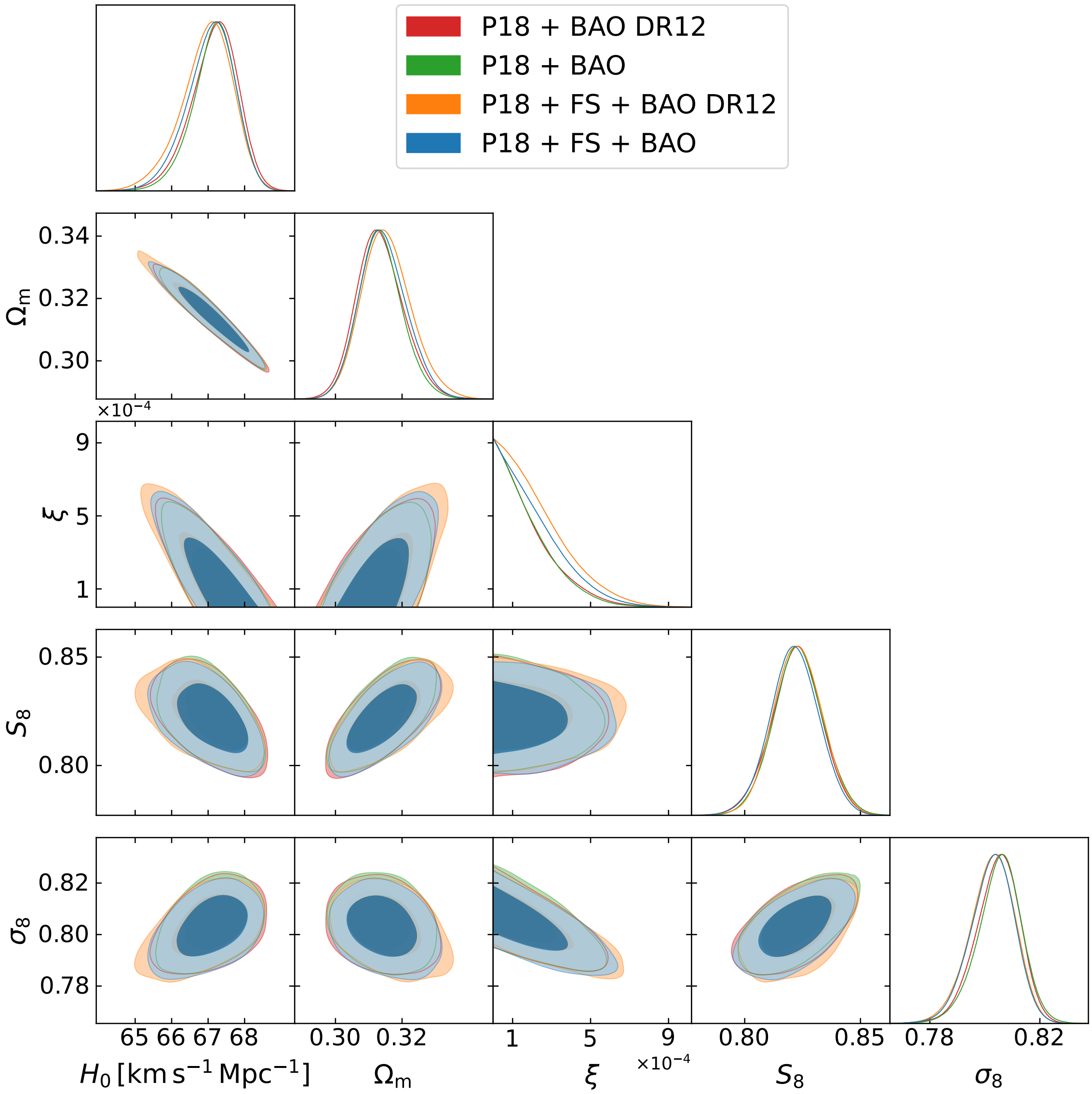

Figure 11. Marginalized joint 68% and 95% C.L. regions 2D parameter space using the CMB P18 data for IG ($F = \xi\sigma^2$) in the phantom branch ($Z = -1$) in combination with BAO from BOSS DR12 (red), BAO from BOSS DR12/SDSS DR7 6dF-MGS/eBOSS (green), FS plus BAO from BOSS DR12 (orange), and FS plus BAO from BOSS DR12/SDSS DR7 6dF-MGS/eBOSS (blue).

References

[1] Supernova Search Team collaboration, *Observational evidence from supernovae for an accelerating universe and a cosmological constant*, Astron. J. **116** (1998) 1009 [astro-ph/9805201] [inSPIRE].

[2] Supernova Cosmology Project collaboration, *Measurements of Ω and Λ from 42 high redshift supernovae*, Astrophys. J. **517** (1999) 565 [astro-ph/9812133] [inSPIRE].

[3] A. Carr et al., *The Pantheon+ analysis: Improving the redshifts and peculiar velocities of Type Ia supernovae used in cosmological analyses*, Publ. Astron. Soc. Austral. **39** (2022) e046 [arXiv:2112.01471] [inSPIRE].

[4] Planck collaboration, *Planck 2018 results. Part I. Overview and the cosmological legacy of Planck*, Astron. Astrophys. **641** (2020) A1 [arXiv:1807.06205] [INSPIRE].

[5] eBOSS collaboration, *Completed SDSS-IV extended Baryon Oscillation Spectroscopic Survey: Cosmological implications from two decades of spectroscopic surveys at the Apache Point Observatory*, Phys. Rev. D **103** (2021) 083533 [arXiv:2007.08991] [INSPIRE].

[6] A. Veropalumbo, F. Marulli, L. Moscardini, M. Moresco and A. Cimatti, *An improved measurement of baryon acoustic oscillations from the correlation function of galaxy clusters at $z \sim 0.3$*, Mon. Not. Roy. Astron. Soc. **442** (2014) 3275 [arXiv:1311.5895] [INSPIRE].

[7] B.D. Sherwin et al., *Two-season Atacama Cosmology Telescope polarimeter lensing power spectrum*, Phys. Rev. D **95** (2017) 123529 [arXiv:1611.09753] [INSPIRE].

[8] W.L.K. Wu et al., *A Measurement of the Cosmic Microwave Background Lensing Potential and Power Spectrum from $500\,\mathrm{deg}^2$ of SPTpol Temperature and Polarization Data*, Astrophys. J. **884** (2019) 70 [arXiv:1905.05777] [INSPIRE].

[9] O. Darwish et al., *The Atacama Cosmology Telescope: A CMB lensing mass map over 2100 square degrees of sky and its cross-correlation with BOSS-CMASS galaxies*, Mon. Not. Roy. Astron. Soc. **500** (2020) 2250 [arXiv:2004.01139] [INSPIRE].

[10] KiDS collaboration, *KiDS-1000 Cosmology: Cosmic shear constraints and comparison between two point statistics*, Astron. Astrophys. **645** (2021) A104 [arXiv:2007.15633] [INSPIRE].

[11] DES collaboration, *Dark Energy Survey Year 3 results: Cosmological constraints from galaxy clustering and weak lensing*, Phys. Rev. D **105** (2022) 023520 [arXiv:2105.13549] [INSPIRE].

[12] R.J. Cooke, M. Pettini and C.C. Steidel, *One Percent Determination of the Primordial Deuterium Abundance*, Astrophys. J. **855** (2018) 102 [arXiv:1710.11129] [INSPIRE].

[13] C. Umiltà, M. Ballardini, F. Finelli and D. Paoletti, *CMB and BAO constraints for an induced gravity dark energy model with a quartic potential*, JCAP **08** (2015) 017 [arXiv:1507.00718] [INSPIRE].

[14] M. Rossi et al., *Cosmological constraints on post-Newtonian parameters in effectively massless scalar-tensor theories of gravity*, Phys. Rev. D **100** (2019) 103524 [arXiv:1906.10218] [INSPIRE].

[15] V. Poulin, T.L. Smith, T. Karwal and M. Kamionkowski, *Early Dark Energy Can Resolve The Hubble Tension*, Phys. Rev. Lett. **122** (2019) 221301 [arXiv:1811.04083] [INSPIRE].

[16] P. Agrawal, F.-Y. Cyr-Racine, D. Pinner and L. Randall, *Rock 'n' Roll Solutions to the Hubble Tension*, arXiv:1904.01016 [INSPIRE].

[17] L. Hart and J. Chluba, *Updated fundamental constant constraints from Planck 2018 data and possible relations to the Hubble tension*, Mon. Not. Roy. Astron. Soc. **493** (2020) 3255 [arXiv:1912.03986] [INSPIRE].

[18] K. Jedamzik and L. Pogosian, *Relieving the Hubble tension with primordial magnetic fields*, Phys. Rev. Lett. **125** (2020) 181302 [arXiv:2004.09487] [INSPIRE].

[19] M. Ballardini, M. Braglia, F. Finelli, D. Paoletti, A.A. Starobinsky and C. Umiltà, *Scalar-tensor theories of gravity, neutrino physics, and the H_0 tension*, JCAP **10** (2020) 044 [arXiv:2004.14349] [INSPIRE].

[20] M. Braglia, M. Ballardini, F. Finelli and K. Koyama, *Early modified gravity in light of the H_0 tension and LSS data*, Phys. Rev. D **103** (2021) 043528 [arXiv:2011.12934] [INSPIRE].

[21] A. Antony, F. Finelli, D.K. Hazra and A. Shafieloo, *Discordances in Cosmology and the Violation of Slow-Roll Inflationary Dynamics*, Phys. Rev. Lett. **130** (2023) 111001 [arXiv:2202.14028] [INSPIRE].

JCAP04(2023)029

[22] L. Knox and M. Millea, *Hubble constant Hunter's guide*, Phys. Rev. D **101** (2020) 043533 [arXiv:1908.03663] [INSPIRE].

[23] E. Di Valentino et al., *Snowmass2021 — Letter of interest cosmology intertwined. Part II. The Hubble constant tension*, Astropart. Phys. **131** (2021) 102605 [arXiv:2008.11284] [INSPIRE].

[24] E. Di Valentino et al., *Cosmology Intertwined. Part III. $f\sigma_8$ and S_8*, Astropart. Phys. **131** (2021) 102604 [arXiv:2008.11285] [INSPIRE].

[25] E. Di Valentino et al., *In the realm of the Hubble tension — a review of solutions*, Class. Quant. Grav. **38** (2021) 153001 [arXiv:2103.01183] [INSPIRE].

[26] L. Perivolaropoulos and F. Skara, *Challenges for ΛCDM: An update*, New Astron. Rev. **95** (2022) 101659 [arXiv:2105.05208] [INSPIRE].

[27] N. Schöneberg, G. Franco Abellán, A. Pérez Sánchez, S.J. Witte, V. Poulin and J. Lesgourgues, *The H_0 Olympics: A fair ranking of proposed models*, Phys. Rept. **984** (2022) 1 [arXiv:2107.10291] [INSPIRE].

[28] P. Shah, P. Lemos and O. Lahav, *A buyer's guide to the Hubble constant*, Astron. Astrophys. Rev. **29** (2021) 9 [arXiv:2109.01161] [INSPIRE].

[29] E. Abdalla et al., *Cosmology intertwined: A review of the particle physics, astrophysics, and cosmology associated with the cosmological tensions and anomalies*, J. High Energy Astrophys. **34** (2022) 49 [arXiv:2203.06142] [INSPIRE].

[30] Planck collaboration, *Planck 2018 results. Part VI. Cosmological parameters*, Astron. Astrophys. **641** (2020) A6 [*Erratum ibid.* **652** (2021) C4] [arXiv:1807.06209] [INSPIRE].

[31] A.G. Riess et al., *A Comprehensive Measurement of the Local Value of the Hubble Constant with $1\,km\,s^{-1}\,Mpc^{-1}$ Uncertainty from the Hubble Space Telescope and the SH0ES Team*, Astrophys. J. Lett. **934** (2022) L7 [arXiv:2112.04510] [INSPIRE].

[32] M. Ballardini, F. Finelli, C. Umiltà and D. Paoletti, *Cosmological constraints on induced gravity dark energy models*, JCAP **05** (2016) 067 [arXiv:1601.03387] [INSPIRE].

[33] J.C. Hill, E. McDonough, M.W. Toomey and S. Alexander, *Early dark energy does not restore cosmological concordance*, Phys. Rev. D **102** (2020) 043507 [arXiv:2003.07355] [INSPIRE].

[34] M. Braglia et al., *Larger value for H_0 by an evolving gravitational constant*, Phys. Rev. D **102** (2020) 023529 [arXiv:2004.11161] [INSPIRE].

[35] M.M. Ivanov et al., *Constraining Early Dark Energy with Large-Scale Structure*, Phys. Rev. D **102** (2020) 103502 [arXiv:2006.11235] [INSPIRE].

[36] K. Rezazadeh, A. Ashoorioon and D. Grin, *Cascading Dark Energy*, arXiv:2208.07631 [INSPIRE].

[37] T.L. Smith, V. Poulin, J.L. Bernal, K.K. Boddy, M. Kamionkowski and R. Murgia, *Early dark energy is not excluded by current large-scale structure data*, Phys. Rev. D **103** (2021) 123542 [arXiv:2009.10740] [INSPIRE].

[38] M. Ballardini, F. Finelli and D. Sapone, *Cosmological constraints on the gravitational constant*, JCAP **06** (2022) 004 [arXiv:2111.09168] [INSPIRE].

[39] T. Simon, P. Zhang, V. Poulin and T.L. Smith, *Updated constraints from the effective field theory analysis of the BOSS power spectrum on early dark energy*, Phys. Rev. D **107** (2023) 063505 [arXiv:2208.05930] [INSPIRE].

[40] E. McDonough, M.-X. Lin, J.C. Hill, W. Hu and S. Zhou, *Early dark sector, the Hubble tension, and the Swampland*, Phys. Rev. D **106** (2022) 043525 [arXiv:2112.09128] [INSPIRE].

[41] A. Gómez-Valent, Z. Zheng, L. Amendola, C. Wetterich and V. Pettorino, *Coupled and uncoupled early dark energy, massive neutrinos, and the cosmological tensions*, Phys. Rev. D **106** (2022) 103522 [arXiv:2207.14487] [INSPIRE].

JCAP04(2023)029

[42] A. Reeves, L. Herold, S. Vagnozzi, B.D. Sherwin and E.G.M. Ferreira, *Restoring cosmological concordance with early dark energy and massive neutrinos?*, *Mon. Not. Roy. Astron. Soc.* **520** (2023) 3688 [arXiv:2207.01501] [INSPIRE].

[43] B. Boisseau, G. Esposito-Farese, D. Polarski and A.A. Starobinsky, *Reconstruction of a scalar tensor theory of gravity in an accelerating universe*, *Phys. Rev. Lett.* **85** (2000) 2236 [gr-qc/0001066] [INSPIRE].

[44] R.R. Caldwell, *A Phantom menace?*, *Phys. Lett. B* **545** (2002) 23 [astro-ph/9908168] [INSPIRE].

[45] J.M. Cline, S. Jeon and G.D. Moore, *The Phantom menaced: Constraints on low-energy effective ghosts*, *Phys. Rev. D* **70** (2004) 043543 [hep-ph/0311312] [INSPIRE].

[46] H.P. Nilles, *Supersymmetry, Supergravity and Particle Physics*, *Phys. Rept.* **110** (1984) 1 [INSPIRE].

[47] M.D. Pollock, *On the Initial Conditions for Superexponential Inflation*, *Phys. Lett. B* **215** (1988) 635 [INSPIRE].

[48] R. Gannouji, D. Polarski, A. Ranquet and A.A. Starobinsky, *Scalar-Tensor Models of Normal and Phantom Dark Energy*, *JCAP* **09** (2006) 016 [astro-ph/0606287] [INSPIRE].

[49] B. Bertotti, L. Iess and P. Tortora, *A test of general relativity using radio links with the Cassini spacecraft*, *Nature* **425** (2003) 374 [INSPIRE].

[50] T. Clifton, J.D. Barrow and R.J. Scherrer, *Constraints on the variation of G from primordial nucleosynthesis*, *Phys. Rev. D* **71** (2005) 123526 [astro-ph/0504418] [INSPIRE].

[51] J. Muller and L. Biskupek, *Variations of the gravitational constant from lunar laser ranging data*, *Class. Quant. Grav.* **24** (2007) 4533 [INSPIRE].

[52] E. Belgacem, A. Finke, A. Frassino and M. Maggiore, *Testing nonlocal gravity with Lunar Laser Ranging*, *JCAP* **02** (2019) 035 [arXiv:1812.11181] [INSPIRE].

[53] D. Alonso, E. Bellini, P.G. Ferreira and M. Zumalacárregui, *Observational future of cosmological scalar-tensor theories*, *Phys. Rev. D* **95** (2017) 063502 [arXiv:1610.09290] [INSPIRE].

[54] M. Ballardini, D. Sapone, C. Umiltà, F. Finelli and D. Paoletti, *Testing extended Jordan-Brans-Dicke theories with future cosmological observations*, *JCAP* **05** (2019) 049 [arXiv:1902.01407] [INSPIRE].

[55] G. Esposito-Farese and D. Polarski, *Scalar tensor gravity in an accelerating universe*, *Phys. Rev. D* **63** (2001) 063504 [gr-qc/0009034] [INSPIRE].

[56] F. Cooper and G. Venturi, *Cosmology and Broken Scale Invariance*, *Phys. Rev. D* **24** (1981) 3338 [INSPIRE].

[57] C. Wetterich, *Cosmologies With Variable Newton's 'Constant'*, *Nucl. Phys. B* **302** (1988) 645 [INSPIRE].

[58] L. Amendola, *Scaling solutions in general nonminimal coupling theories*, *Phys. Rev. D* **60** (1999) 043501 [astro-ph/9904120] [INSPIRE].

[59] F. Finelli, A. Tronconi and G. Venturi, *Dark Energy, Induced Gravity and Broken Scale Invariance*, *Phys. Lett. B* **659** (2008) 466 [arXiv:0710.2741] [INSPIRE].

[60] J. Lesgourgues, *The Cosmic Linear Anisotropy Solving System (CLASS). Part I. Overview*, arXiv:1104.2932 [INSPIRE].

[61] D. Blas, J. Lesgourgues and T. Tram, *The Cosmic Linear Anisotropy Solving System (CLASS). Part II. Approximation schemes*, *JCAP* **07** (2011) 034 [arXiv:1104.2933] [INSPIRE].

JCAP04(2023)029

[62] B. Audren, J. Lesgourgues, K. Benabed and S. Prunet, *Conservative Constraints on Early Cosmology: an illustration of the Monte Python cosmological parameter inference code*, *JCAP* **02** (2013) 001 [arXiv:1210.7183] [INSPIRE].

[63] T. Brinckmann and J. Lesgourgues, *MontePython 3: boosted MCMC sampler and other features*, *Phys. Dark Univ.* **24** (2019) 100260 [arXiv:1804.07261] [INSPIRE].

[64] PLANCK collaboration, *Planck 2018 results. Part V. CMB power spectra and likelihoods*, *Astron. Astrophys.* **641** (2020) A5 [arXiv:1907.12875] [INSPIRE].

[65] PLANCK collaboration, *Planck 2018 results. Part VIII. Gravitational lensing*, *Astron. Astrophys.* **641** (2020) A8 [arXiv:1807.06210] [INSPIRE].

[66] H. Gil-Marín et al., *The clustering of galaxies in the SDSS-III Baryon Oscillation Spectroscopic Survey: RSD measurement from the LOS-dependent power spectrum of DR12 BOSS galaxies*, *Mon. Not. Roy. Astron. Soc.* **460** (2016) 4188 [arXiv:1509.06386] [INSPIRE].

[67] G. D'Amico, L. Senatore and P. Zhang, *Limits on wCDM from the EFTofLSS with the PyBird code*, *JCAP* **01** (2021) 006 [arXiv:2003.07956] [INSPIRE].

[68] BOSS collaboration, *The clustering of galaxies in the completed SDSS-III Baryon Oscillation Spectroscopic Survey: cosmological analysis of the DR12 galaxy sample*, *Mon. Not. Roy. Astron. Soc.* **470** (2017) 2617 [arXiv:1607.03155] [INSPIRE].

[69] F. Beutler et al., *The 6dF Galaxy Survey: Baryon Acoustic Oscillations and the Local Hubble Constant*, *Mon. Not. Roy. Astron. Soc.* **416** (2011) 3017 [arXiv:1106.3366] [INSPIRE].

[70] A.J. Ross, L. Samushia, C. Howlett, W.J. Percival, A. Burden and M. Manera, *The clustering of the SDSS DR7 main Galaxy sample. Part I. A 4 per cent distance measure at $z = 0.15$*, *Mon. Not. Roy. Astron. Soc.* **449** (2015) 835 [arXiv:1409.3242] [INSPIRE].

[71] V. de Sainte Agathe et al., *Baryon acoustic oscillations at $z = 2.34$ from the correlations of Lyα absorption in eBOSS DR14*, *Astron. Astrophys.* **629** (2019) A85 [arXiv:1904.03400] [INSPIRE].

[72] M. Blomqvist et al., *Baryon acoustic oscillations from the cross-correlation of Lyα absorption and quasars in eBOSS DR14*, *Astron. Astrophys.* **629** (2019) A86 [arXiv:1904.03430] [INSPIRE].

[73] A. Cuceu, J. Farr, P. Lemos and A. Font-Ribera, *Baryon Acoustic Oscillations and the Hubble Constant: Past, Present and Future*, *JCAP* **10** (2019) 044 [arXiv:1906.11628] [INSPIRE].

[74] PAN-STARRS1 collaboration, *The Complete Light-curve Sample of Spectroscopically Confirmed SNe Ia from Pan-STARRS1 and Cosmological Constraints from the Combined Pantheon Sample*, *Astrophys. J.* **859** (2018) 101 [arXiv:1710.00845] [INSPIRE].

[75] O. Pisanti et al., *PArthENoPE: Public Algorithm Evaluating the Nucleosynthesis of Primordial Elements*, *Comput. Phys. Commun.* **178** (2008) 956 [arXiv:0705.0290] [INSPIRE].

[76] R. Consiglio, P.F. de Salas, G. Mangano, G. Miele, S. Pastor and O. Pisanti, *PArthENoPE reloaded*, *Comput. Phys. Commun.* **233** (2018) 237 [arXiv:1712.04378] [INSPIRE].

[77] M. Zumalacarregui, *Gravity in the Era of Equality: Towards solutions to the Hubble problem without fine-tuned initial conditions*, *Phys. Rev. D* **102** (2020) 023523 [arXiv:2003.06396] [INSPIRE].

[78] J. Solà Peracaula, A. Gómez-Valent, J. de Cruz Pérez and C. Moreno-Pulido, *Brans-Dicke cosmology with a Λ-term: a possible solution to ΛCDM tensions*, *Class. Quant. Grav.* **37** (2020) 245003 [arXiv:2006.04273] [INSPIRE].

[79] M. Ballardini and F. Finelli, *Type Ia supernovae data with scalar-tensor gravity*, *Phys. Rev. D* **106** (2022) 063531 [arXiv:2112.15126] [INSPIRE].

[80] J. Garriga and V.F. Mukhanov, *Perturbations in k-inflation*, *Phys. Lett. B* **458** (1999) 219 [hep-th/9904176] [INSPIRE].

[81] M. Gasperini and G. Veneziano, *The Pre-big bang scenario in string cosmology*, *Phys. Rept.* **373** (2003) 1 [hep-th/0207130] [INSPIRE].

[82] N. Arkani-Hamed, H.-C. Cheng, M.A. Luty and S. Mukohyama, *Ghost condensation and a consistent infrared modification of gravity*, *JHEP* **05** (2004) 074 [hep-th/0312099] [INSPIRE].

[83] A. Nicolis, R. Rattazzi and E. Trincherini, *The Galileon as a local modification of gravity*, *Phys. Rev. D* **79** (2009) 064036 [arXiv:0811.2197] [INSPIRE].

[84] C. Deffayet, G. Esposito-Farese and A. Vikman, *Covariant Galileon*, *Phys. Rev. D* **79** (2009) 084003 [arXiv:0901.1314] [INSPIRE].

[85] F.P. Silva and K. Koyama, *Self-Accelerating Universe in Galileon Cosmology*, *Phys. Rev. D* **80** (2009) 121301 [arXiv:0909.4538] [INSPIRE].

[86] T. Kobayashi, *Cosmic expansion and growth histories in Galileon scalar-tensor models of dark energy*, *Phys. Rev. D* **81** (2010) 103533 [arXiv:1003.3281] [INSPIRE].

[87] A. Ferrari et al., *Constraints on Galileon scalar-tensor theories with standard and nonstandard kinetic term*, in preparation (2023).

[88] C.-P. Ma and E. Bertschinger, *Cosmological perturbation theory in the synchronous and conformal Newtonian gauges*, *Astrophys. J.* **455** (1995) 7 [astro-ph/9506072] [INSPIRE].

[89] D. Paoletti, M. Braglia, F. Finelli, M. Ballardini and C. Umiltà, *Isocurvature fluctuations in the effective Newton's constant*, *Phys. Dark Univ.* **25** (2019) 100307 [arXiv:1809.03201] [INSPIRE].

JCAP04(2023)029